ELSEVIER

Contents lists available at ScienceDirect

Journal of Molecular Spectroscopy

journal homepage: www.elsevier.com/locate/yjmsp





The eight lowest-energy vibrational states of benzonitrile: analysis of Coriolis and Darling-Dennison couplings by millimeter-wave and far-infrared spectroscopy

Maria A. Zdanovskaia ^a, Marie-Aline Martin-Drumel ^{b,c}, Zbigniew Kisiel ^d, Olivier Pirali ^{b,c}, Brian J. Esselman ^a, R. Claude Woods ^{a,*}, Robert J. McMahon ^{a,*}

- ^a Department of Chemistry, University of Wisconsin–Madison, Madison, WI 53706, USA
- ^b AILES Beamline, Synchrotron SOLEIL, l'Orme des Merisiers, Saint-Aubin, 91192 Gif-sur-Yvette cedex, France
- ^c Université Paris-Saclay, CNRS, Institut des Sciences Moléculaires d'Orsay, 91405 Orsay, France
- d Institute of Physics, Polish Academy of Sciences, Al. Lotników 32/46, 02-668 Warszawa, Poland

ARTICLE INFO

Keywords: Rotationally resolved infrared spectroscopy Rotational spectroscopy Coriolis coupling Darling-Dennison coupling Anharmonicity constants Interstellar molecule Astrochemistry

ABSTRACT

A combination of millimeter-wave and high-resolution infrared data is used to analyze the eight lowest-energy vibrational states of benzonitrile (C_6H_5CN , $C_{2\nu}$, $\mu_a=4.5$ D), a benzene derivative recently detected in the interstellar medium. The overtone states $v_{22}=2$ and $v_{33}=2$, combination state $v_{22}=1$, $v_{33}=1$, and fundamental states $v_{21} = 1$ and $v_{15} = 1$ are studied for the first time by rotationally resolved spectroscopy. The three former states form a Coriolis- and Darling-Dennison-coupled triad of interacting states for which the coupling terms and highly precise, deperturbed energy separations have been measured. The use of sub-millimeter and far-infrared data together enabled the determination of the purely rotational and coupling parameters for the six lowestenergy vibrationally excited states of benzonitrile, along with their highly precise energies ($E_{22} = 141.4810252$ (57) cm⁻¹, $E_{33} = 160.5891953$ (47) cm⁻¹, $E_{2\times22} = 282.6295417$ (83) cm⁻¹, $E_{22+33} = 302.5795909$ (87) cm⁻¹, $E_{2\times33} = 321.4923856$ (77) cm⁻¹, $E_{21} = 372.257993$ (10) cm⁻¹). These energies, the resultant experimental anharmonicity constants ($x_{22,22} = -0.1663 \text{ cm}^{-1}$, $x_{33,33} = 0.1570 \text{ cm}^{-1}$, and $x_{22,33} = 0.4909$ cm⁻¹), and semi-experimental harmonic frequencies ($\omega_{22} = 142.9 \text{ cm}^{-1}$ and $\omega_{33} = 161.0 \text{ cm}^{-1}$) for the ν_{22} and ν_{33} states are compared to CCSD(T)/ANO1 predicted values. The spectroscopic and coupling constants determined in this work for the vibrational ground state, the two lowest-energy fundamental states, and the corresponding first overtone and combination states successfully predict experimental frequencies down to 8 GHz. Particularly for the vibrationally excited states, the ability to predict transition frequencies so far outside the frequency region in which the constants were determined confirms that the rotational and distortion constants, as well as the coupling terms, are determined reasonably close to their true values. The ability to accurately extrapolate also demonstrates the suitability of the determined constants as the basis for extraterrestrial identification and examination of these vibrational states of benzonitrile.

1. Introduction

The first astronomical detection of an aromatic molecule – the detection of cyclopropenylidene [1,2] – occurred nearly 40 years ago. Initial evidence of interstellar benzene [3] and the detection of cyclopropenone [4] followed in the early 2000's. In a dramatic breakthrough for the astrochemical detection of aromatic species, benzonitrile was recently detected toward Taurus Molecular Cloud 1 (TMC-1), providing the first direct evidence of a substituted, six-membered aromatic

compound in the interstellar medium [5]. This important detection was quickly followed by those of aromatic (cyanonaphthalenes [7], indene, ethynyl cyclopropenylidene [8]), and non-aromatic (cyano-1,3-cyclopentadiene [6], cyclopentadiene [8]) molecules in TMC-1, as well as cyclopropenylidene on Titan [9]. Half of these latest radioastronomical detections are aided by a strong, permanent dipole moment associated with the nitrile moiety (R-C=N). These ecent successes inspire a renewed effort to provide radioastronomers with the accurate spectral data required for further new identifications of polar organic species

E-mail addresses: rcwoods@wisc.edu (R.C. Woods), robert.mcmahon@wisc.edu (R.J. McMahon).

^{*} Corresponding authors.

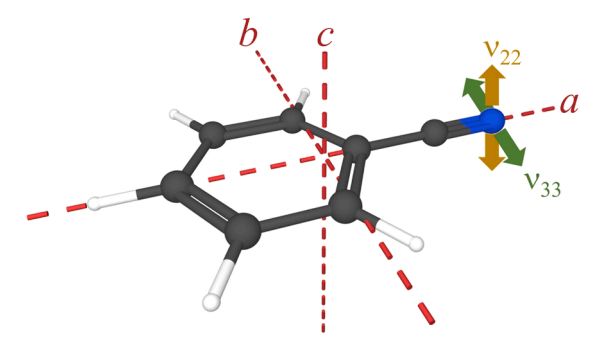


Fig. 1. Benzonitrile with principal inertial axes and representation of nitrogenatom motion for ν_{22} and ν_{33} vibrational modes.

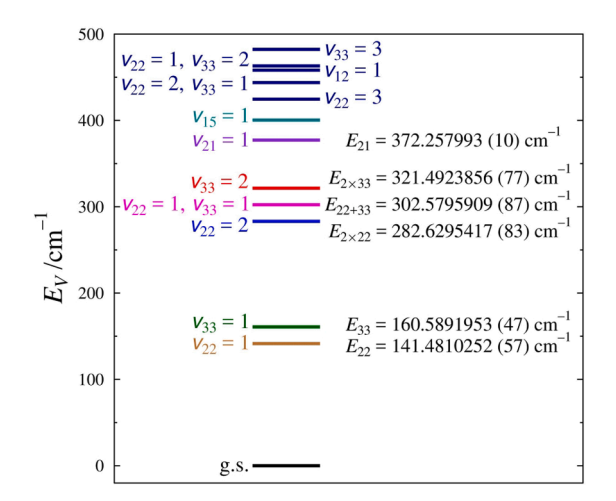


Fig. 2. The vibrational energy levels of benzonitrile below 500 cm⁻¹, drawn from the anharmonic values of the CCSD(T)/ANO1 calculation. The denoted experimental energies result from the high-resolution infrared and perturbation analysis of the present work (*vide infra*). States colored in navy are not examined in this work; all states lower in energy are examined this work.

[10,11].

The confirmation of benzonitrile's ($C_6\mathrm{H}_5\mathrm{CN}$, $C_{2\nu}$, $\kappa=-0.85$, $\mu_a=4.5~\mathrm{D}$ [12]) presence in extraterrestrial environments is particularly exciting to the scientific community. Several studies established its plausibility [13–17], including the crossed molecular beam collision experiment of Balucani *et al.* that demonstrated generation of benzonitrile from cyano radical and benzene *via* a barrierless reaction that is favorable by 95 kJ/mol [14]. Given the presence of benzene [3] and cyano radical [18] in the ISM, the interstellar presence of benzonitrile seemed likely. Numerous studies examined benzonitrile in the infrared (IR) [19,20], centimeter-wave, [5,12,21–26], and millimeter-wave regions [27,28]. It was only recently, however, that the vibrationally excited states were examined in the millimeter-wave region and the Coriolis coupling between the two lowest-energy fundamentals was analyzed [28].

Benzonitrile is among numerous examples of molecules exhibiting vibrationally excited-state couplings successfully analyzed via either rotational or high-resolution infrared spectroscopy [10,11,29–38]. Our previous work on benzonitrile [28] updated the spectroscopic constants using millimeter-wave data up to 360 GHz and analyzed, for the first time, the Coriolis-coupled dyad of its two lowest-energy fundamental states, v_{22} (141 cm⁻¹ [20,39], B_1 symmetry) and v_{33} (163 cm⁻¹ [20,39], B_2 symmetry). The two fundamentals (represented on the structure of benzonitrile in Fig. 1) are bends of the nitrile group with respect to the ring – v_{22} is the out-of-plane bend perpendicular to the plane of the aromatic ring, while v_{33} is the corresponding in-plane bend. In that

work, we were able to determine the a-type Coriolis coupling term, G_a , as well as several higher-order coupling terms and a highly precise energy separation between the two fundamentals.

The study of coupled states has the potential not only to determine the most precise energy separations of any method currently available, but also to help understand various quantum—mechanical phenomena [10,11,28,32,36,38,40,41]. Meanwhile, the ability to accurately predict vibrationally excited-state spectra of a given molecule across a wide frequency range enables their extraterrestrial detection, like that of their ground state. In turn, such detections can help to provide additional confirmation of the presence of the molecule, eliminate "unknown" or unassigned transitions in an observed survey spectrum [42], and offer insight into the environment where the molecule is detected (or not detected). Since transition intensities are linked to abundance, vibrational energies, and temperature, they may provide additional means to estimate properties such as temperatures or molecular abundance in distant regions [31,43–45].

In the present study, we report several advances in the spectroscopic analysis of benzonitrile: (i) we update the spectroscopic constants of the ground vibrational state by recording and analyzing transitions in the 130–230 GHz region, (ii) we provide a computationally predicted value of the centrifugal distortion constan Φ_K , which could not be determined experimentally, (iii) we analyze the $v_{22} = 2$; $v_{22} = 1$, $v_{33} = 1$; and $v_{33} = 2$ Coriolis- and Darling-Dennison-coupled triad (Fig. 2) and report here for the first time their rotational, centrifugal distortion, and coupling parameters, (iv) we report single-state (isolated) spectroscopic parameters for the next higher-energy fundamentals, ν_{21} and ν_{15} , (v) we describe an analysis of the six lowest-energy vibrational states, which have been combined into a single, multi-state fit in which the ground state is connected to the v_{22} - v_{33} dyad through high-resolution infrared measurements, and the latter is linked to the triad states through related hotbands. The combination of infrared data and precise coupling analysis via millimeter-wave data enabled the determination of a highly precise ladder of vibrational energies for benzonitrile.

2. Experimental methods

Samples of benzonitrile were purchased from commercial sources and used without further purification for all measurements. Collection of the 103–136 GHz, 185–207 GHz, and 250–360 GHz spectral portions has been described previously [28]. An additional benzonitrile spectral segment covering the 130–230 GHz frequency region using pressures of 2–6 mTorr and at approximately - 50 $^{\circ}\text{C}$ was collected in this study using the Madison broadband spectrometer [32,46]. Additional data in the 8–18 GHz frequency range were collected on a modified waveguide Fourier-transform microwave spectrometer [47] that was originally constructed in the Kiel laboratory [48,49] and relocated to Warsaw.

High-resolution far-infrared spectra were collected in the 65-695 cm⁻¹ frequency region with a pressure of 58 mTorr (77 μbar) using synchrotron radiation extracted by the AILES beamline of the SOLEIL synchrotron facility. The radiation was focused onto the entrance iris (set to a 2 mm aperture) of a Bruker IFS 125 FT interferometer equipped with a 6 µm Mylar-silicon composite beamsplitter and a helium-cooled silicon bolometer [50]. The interferometer was continuously evacuated to 10^{-5} mbar, limiting the absorption of atmospheric water. Benzonitrile was injected into a White-type multipass cell adjusted to a 150 m optical path length [51] and isolated from the interferometer by ~ 50 μm-thick polypropylene windows. The spectrum consists of 340 scans recorded at the highest resolution of the instrument ($\sim 0.001~\text{cm}^{-1}$ according to the Bruker definition). The interferogram was processed with an 8 times post-zerofilling and without any apodization. An empty cell reference spectrum was recorded at a resolution of 0.5 cm⁻¹ (100 scans) to allow for baseline compensation. The high-resolution infrared spectrum of benzonitrile was calibrated using residual water and CO₂ peaks, whose reference frequencies were obtained from literature [52–54].

In addition to the AABS suite for spectral analysis [55,56], the

Table 1Experimental and computational spectroscopic constants for the ground vibrational state of benzonitrile (A-Reduced Hamiltonian, I^r Representation).

	2018 Work ^a	Current Work, Single-State ^{b,c}	Calc.d	Current Work, Multi-State ^c e
A ₀ (MHz)	5655.265371 (75)	5655.265428 (82)	5616.	5655.25847 (43)
B_0 (MHz)	1546.8757804 (76)	1546.8757715 (80)	1535.	1546.875595 (36)
C_0 (MHz)	1214.4040772 (67)	1214.4040832 (69)	1205.	1214.404340 (28)
Δ_J (kHz)	0.0452653 (27)	0.0452858 (14)	0.0437	0.0452768 (31)
Δ_{JK} (kHz)	0.937906 (27)	0.937983 (20)	0.923	0.937947 (33)
Δ_K (kHz)	0.24234 (77)	0.24411 (75)	0.241	0.22097 (45)
δ_J (kHz)	0.01101589 (73)	0.01101116 (54)	0.0106	0.0110045 (14)
δ_K (kHz)	0.609088 (74)	0.609187 (65)	0.593	0.608023 (94)
Φ_J (Hz)	0.00000051 (22)	0.000002486 (60)	0.00000230	0.00000228 (12)
Φ_{JK} (Hz)	0.0015435 (46)	0.0015586 (41)	0.00149	0.0016099 (57)
Φ_{KJ} (Hz)	-0.007849 (17)	-0.007863 (16)	-0.00761	-0.008080 (25)
Φ_K (Hz)	[0.0]	[0.0066915]	0.0066915	[0.0066915]
ϕ_J (Hz)	0.000001412 (38)	0.000001159 (26)	0.0000110	0.000001137 (58)
ϕ_{JK} (Hz)	0.0007431 (30)	0.0007398 (24)	0.000755	0.0007131 (43)
ϕ_K (Hz)	0.007106 (76)	0.007480 (67)	0.00712	0.008436 (93)
L_J (μ Hz)	0.0000585 (56)	[0.0]		[0.0]
L_{JJK} (μ Hz)	-0.002085 (52)	-0.002198 (39)		-0.002373(69)
L_{JK} (μ Hz)	[0.0]	[0.0]		[0.0]
L_{KKJ} (μ Hz)	-0.0428 (18)	-0.0464 (18)		-0.0441 (28)
L_K (μHz)	4.468 (90)	4.501 (78)		5.496 (65)
χ_{aa} (MHz)	-4.23755 (27)	-4.23755 (30)		
χ_{bb} (MHz)	2.28872 (38)	2.28872 (54)		
$\Delta_i (u\mathring{A}^2)^f$	0.080084 (3)	0.080081 (3)	0.081182^{g}	0.079846 (14)
$N_{ m lines}^{ m h}$	4073 / 0	5819 / 0		5584 / 8843 ⁱ
$\sigma_{\mathrm{fit}}^{}}$	0.025 MHz	0.028 MHz		$0.031~\mathrm{MHz} \ / \ 0.0002~\mathrm{cm}^{-1}$

^a As reported in Ref. [28], including transitions from literature data [5,23,24,26,27].

Loomis-Wood for Windows program was used for infrared spectral visualization and assignment [57], and the PIFORM, PISLIN, PMIXC, PLANM, and AC programs were used for analysis and generation of various plots [58,59]. Least-squares fitting and spectral predictions were carried out using Pickett's SPFIT/SPCAT [60]. In the least-squares fits, we assumed uniform frequency measurement uncertainty of 50 kHz for all measurements from the Madison and Warsaw spectrometers, uncertainties of 0.0002 cm⁻¹ (~6 MHz) for all measurements from the SOLEIL Synchrotron, and uncertainties specified by the respective authors for the literature data. In the case where such a value was not given (ref. [26]) we assumed an uncertainty of 5 kHz, which resulted in weighted, root mean square (RMS) deviation for this subset that was similar to those of the other comparable literature data subsets.

3. Computational methods

A developmental version of the CFOUR program [61] was used for all calculations reported herein. The geometry was optimized at the CCSD (T)/ANO1 level of theory using analytic gradients with the frozen core approximation. Anharmonic vibrational frequencies, vibration–rotation interaction constants (α_i values, B_v - B_0), and Coriolis-coupling (ζ) values were predicted using an anharmonic VPT2 calculation at the same level of theory *via* calculation of cubic and quartic force constants using analytic second derivatives at displaced points [62,63]. A magnetic calculation was completed using the same level of theory to provide the electron-mass correction for the computed inertial defect. The Darling-Dennison interaction term and anharmonic energies of the $v_{22}=2$ and

 $v_{33} = 2$ overtone states were predicted using the *xguinea* module of CFOUR. A description of the use of *xguinea* and all computational output files can be found in the supplementary materials.

4. Analysis of rotational spectra

4.1. Ground state

The ground-state benzonitrile spectrum has previously been analyzed in various spectral regions [5,12,21-27]. In the present work, we have incorporated over 1700 transitions from the newly measured spectral region into the least-squares fit data. Since this spectral region is between the previous low and high spectral segments, the J and K_a quantum number ranges remain nearly the same as in the 2018 work. The resultant, updated spectroscopic constants are the result of a global fit of hyperfine-resolved and unresolved data. The CCSD(T)/ANO1 VPT2 calculation enabled prediction of the sextic constants, which had not been previously available. Since Φ_K could not be determined in the 2018 work, its value was held constant at zero at that time. Presumably, however, a predicted constant would be closer to its actual value, making all of the fitted parameters more physically meaningful. Therefore, we have updated the ground-state constants with the predicted value of Φ_{K} . These constants are provided for comparison in Table 1 alongside the previously determined constants, the computed constants, and those determined in a multi-state least-squares fit including high-resolution infrared data. Although the rotational constants of the heavy-atom isotopologues have been reported in the course

^b Global fit to the present, expanded mm-wave measurements and the available literature data [5,23,24,26,27].

^c Constants that could not be determined are held constant at the CCSD(T)/ANO1 value.

d Evaluated at CCSD(T)/ANO1.

^e Global fit of the present, expanded mm-wave measurements, literature data [24,27] excluding hyperfine-resolved transitions, and new high-resolution infrared data in a combined least-squares fit with $\nu_{22}=1$; $\nu_{33}=1$; $\nu_{22}=2$; $\nu_{22}=1$, $\nu_{33}=1$; and $\nu_{33}=2$.

f Inertial defect using B_0 values, $\Delta_i = I_c - I_a - I_b$.

^g Rotational constants used to determine computational inertial defect include computed corrections for the effects of electron-mass distribution.

h Number of fitted transition frequencies (millimeter-wave / IR).

ⁱ Infrared data includes $v_{22} = 1 \leftarrow \text{g.s.}$ and $v_{33} = 1 \leftarrow \text{g.s.}$ transitions.

^j Values presented in MHz are for millimeter-wave data; value in cm⁻¹ is for IR data.

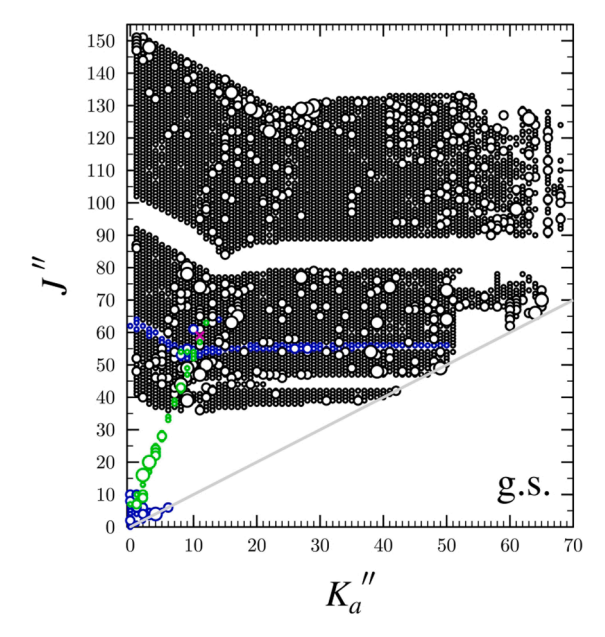


Fig. 3. Data distribution plot for the global fit of combined spectroscopic data for the vibrational ground state of benzonitrile. The size of the plotted symbol is proportional to the value of $|(f_{\rm obs.} - f_{\rm calc.})/\delta f|$, where δf is frequency measurement uncertainty, and all values are smaller than 3. Black circles denote R-branch transitions from the present work, blue circles mark R-branch transitions from literature data [5,23,24,26,27], and green circles mark Q-branch transitions from literature data. A magenta cross identifies a single, literature P-branch transition.

of several substitution structures [23,24,64] and a B3LYP semiexperimental equilibrium structure [65], we have been unable to observe these isotopologues at natural abundance in our frequency region due to the high spectral density.

The updated spectroscopic constants based on a single-state leastsquares fit of the ground vibrational state of benzonitrile are nearly unchanged relative to those reported in 2018. While the value of L_J could no longer be determined, all of the fitted constants except for Φ_J and ϕ_J are within 1% of their respective 2018 and updated values. The 2018 value of Φ_I is 80% smaller than the updated value and that of ϕ_I is 22% different. These changes occur as a consequence of updating the sextic distortion constant Φ_K from a value of zero in the earlier study to a computed value in this work. The values of the inertial defect (Δ_i) agree within their uncertainty. The agreement of the computed constants with their experimental values is highly satisfactory, which serves to validate the accuracy of the calculation and the physical meaningfulness of the experimental centrifugal distortion constants. Each of the rotational constants is within 0.8% of the experimental values, and all of the distortion constants are within 5.1%. As mentioned in the 2018 work, the computed inertial defect, which is based on B_0 values corrected from the equilibrium constants for only the vibration-rotation interaction, is overpredicted (0.093 uÅ²). Additional correction for electron-mass distribution, as previously suggested [28,65], brings the computed inertial defect (0.081 uÅ²) in much closer agreement with the experimental value (0.080081 (3) $uÅ^2$). Table 1 also provides a comparison to the spectroscopic constants of the ground state fitted in a multi-state least-squares fit involving $v_{22} = 1$; $v_{33} = 1$; $v_{22} = 2$; $v_{22} = 1$, $v_{33} = 1$; and $v_{33} = 2$ and linked to the dyad of the two fundamental states via infrared transitions. It is expected that these spectroscopic constants, particularly some of the distortion constants, are somewhat less physically meaningful than those determined in the single-state least-squares fit. Excited-state rotational and centrifugal constants change approximately linearly as a function of vibrational quantum number. Due to the inability to satisfactorily determine some of the excited-state distortion constants, however, they were held constant at the best estimate of their

Table 2Summary of millimeter-wave and high-resolution infrared data subsets used in least-squares fits of the present work for benzonitrile.

	$N_{ m lines}^{ m a}$	${\sigma_{ m fit}}^{ m b}$	J range ^c	K_a range c	Frequency range ^d
Millimeter-wave	e data				
g.s. ^e	5815	0.028	0 - 153	0 - 68	2760 - 374,509
$v_{22} = 1$	3001	0.035	36 - 147	0 - 47	103,163 -
					359,867
$v_{33} = 1$	2933	0.037	36 - 147	0 - 47	103,226 -
					359,917
$v_{22}=2$	3385	0.038	17 - 146	0 - 50	103,324 -
					365,238
$v_{22} = 1$, $v_{33} =$	3161	0.053	36 - 147	0 - 48	103,187 –
1					371,670
$v_{33}=2$	3152	0.045	35 - 147	0 - 48	103,227 –
					359,759
$ u_{21}=1$	1992	0.041	36 - 147	0 - 40	103,167 –
					359,590
$v_{15}=1$	1642	0.042	36 - 142	0 - 40	105,607 –
					358,518
Infrared data					
$v_{22} = 1 \leftarrow 0$	2373	0.00022	5 – 160	0 – 44	122.96 – 155.12
$v_{33} = 1 \leftarrow 0$	6470	0.00021	3 - 160	0 – 49	141.18 – 191.56
$v_{22} = 2 \leftarrow 1$	1273	0.00018	5 – 106	0 – 44	124.00 - 153.30
$v_{33} = 2 \leftarrow 1$	1139	0.00034	15 - 129	0 – 46	149.07 – 187.87
$v_{21} = 1 \leftarrow 0$	1072	0.00017	7 – 114	0 - 44	353.25 - 386.06

^a Number of fitted transition frequencies.

values currently available - the corresponding ground-state value. As a result, in the data set with excited-state constants held at their groundstate values, it is likely that the ground-state constants were somewhat distorted to account for the changes actually occurring in the distortion constants. Nevertheless, the ground-state rotational constants fitted in the multi-state model are within 0.0002% of those determined in the single-state fit, the quartic distortion constants are within 0.2% (except Δ_K , which differs by 9.5%), the sextic constants are within 8.3% (except ϕ_K , which differs by 12.8%), and the fitted octic constants are within 8% (except L_K , which differs by 22.1%). Indeed, there is a clear pattern that A_0 and the purely K-dependent terms change the most, and this may reflect the fact that these constants are most correlated with the a-type Coriolis-coupling terms of three dyads in the multi-state fit. As a result of this convolution, none of the listed distortion constants was determined for the excited states in the multi-state fit, and therefore these constants were the most affected in the ground state. These changes are also reflected in the smaller value of the inertial defect relative to the singlestate fit value. The data distribution plot from the single-state fit showing the range of measured J and K_a values in the updated data is presented in Fig. 3, and these same transitions were used in the multistate fit. A summary of the infrared and millimeter-wave data for all vibrational states presented in this work is provided in Table 2. Although multi-state least-squares fits, in which the ground-state parameters were held constant at their single-state values and various sets of excited-state parameters were allowed to be fit, were attempted, none of these fits were able to converge.

4.2. The excited states: Coriolis-coupled dyad and corresponding overtone and combination state triad

The millimeter-wave spectra of the ground vibrational state and two

 $^{^{\}rm b}$ RMS error provided in MHz for millimeter-wave data and in ${\rm cm}^{-1}$ for IR data.

^c Values of J and K_a are the lowest and highest values reported in the data set, irrespective of whether they appear in the lower or upper rotational energy level.

 $^{^{\}rm d}$ Frequency range provided in MHz for millimeter-wave data and in ${\rm cm}^{-1}$ for IR data.

^e Ground state data reported for single-state fit ground state reported for single-state fit with literature data, including hyperfine-resolved transitions [5,23,24,26,27].

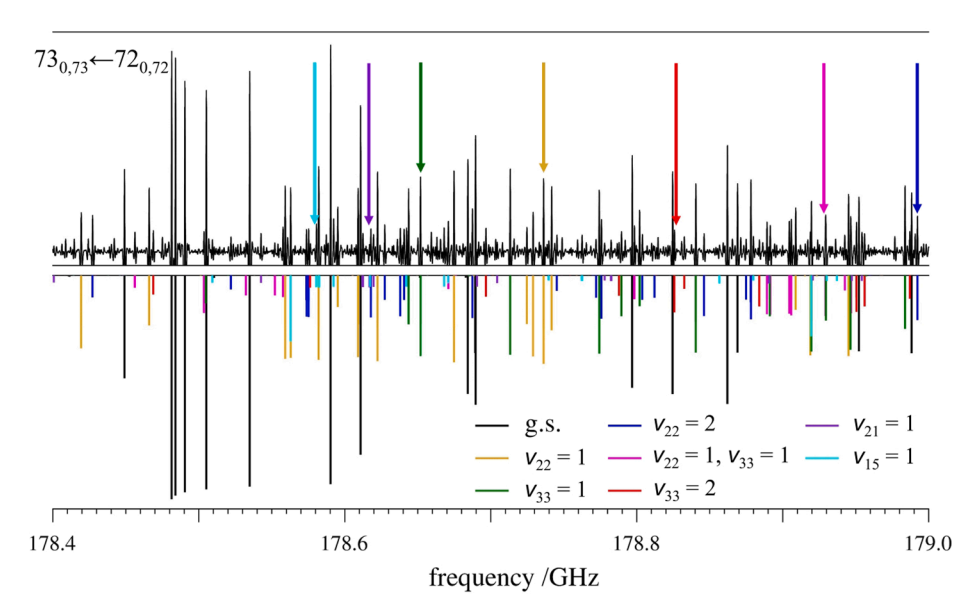


Fig. 4. Benzonitrile rotational spectrum from 178.4 to 179.0 GHz (top) and stick spectrum of the ground vibrational state and seven vibrationally excited states (bottom). The strongest transitions belong to the n=2, type-II⁺ bands [66,67]. The bandheads in this frequency region start at the $73_{0,73} \leftarrow 72_{0,72}$ transition of each vibrational state. The ground-state transition is near 178.48 GHz, and the corresponding transition for each excited state is marked with an arrow in the corresponding color. Numerous yet-to-be analyzed transitions belonging to other vibrational satellites are visible.

lowest-energy fundamental states, ν_{22} and ν_{33} , have been described in detail previously [28], and all of the states described herein follow similar patterns. Each of the observed vibrational state spectra exhibits typical oblate-type band structure, where the first peak in the visual series is composed of two degenerate transitions with $K_a=0$ and 1 and equal values of K_c . Subsequent peaks in the band have increasing values of K_a and decreasing values of J. At higher values of J are transitions sharing the same value of J are even higher J and J are even higher J and J are even higher J and J and J are even higher J and J are even higher J and J and J are even higher J and J are even higher frequencies from the corresponding ground-state bandhead, as shown in Fig. 4.

Purely rotational transitions for the $v_{22}=2$; $v_{22}=1$, $v_{33}=1$; and $v_{33}=2$ vibrational satellites were initially located by extrapolating the $K_a=0$ frequencies from the ground-state and fundamental frequencies. In this case, this method of direct frequency extrapolation predicts the low- K_a transition frequencies more accurately than prediction using experimentally extrapolated and predicted spectroscopic constants. Once an initial set of low- K_a transitions had been measured and assigned, the triad states were combined into a coupled-state fit. Rotational constants

and distortion constants that were determined for the ground state and dyad of fundamentals were extrapolated to provide initial estimates for the corresponding triad state. Distortion constants that could not be extrapolated were held constant at the corresponding ground-state value from the single-state model. The initial predictions of the energy separations between $v_{22}=2$ and the two higher-energy triad states were based on the experimentally determined energy separation between $v_{22}=1$ and $v_{33}=1$. The initial estimate of $w_{33}=1$, the initial estimate of $w_{33}=1$ and $w_{33}=1$. The initial estimate of $w_{33}=1$ and $w_{33}=1$ are the initial estimate of $w_{33}=1$ and $w_{33}=1$. The initial estimate of $w_{33}=1$ and $w_{33}=1$ are the initial estimate of $w_{33}=1$ and $w_{33}=1$ and $w_{33}=1$ and $w_{33}=1$ are the initial estimate of $w_{33}=1$ and $w_{33}=1$. The initial estimate of $w_{33}=1$ and $w_{33}=1$ are the initial estimate of $w_{33}=1$ and $w_{33}=1$ are the initial estimate of $w_{33}=1$ and $w_{33}=1$. The initial estimate of $w_{33}=1$ and $w_{33}=1$ are the initial estimate of $w_{33}=1$ and $w_{33}=1$ and $w_{33}=1$ and $w_{33}=1$ and $w_{33}=1$ are the initial estimate of $w_{33}=1$ and $w_{33}=1$ and $w_{33}=1$ and $w_{33}=1$ are the initial estimate of $w_{33}=1$ and w_{3

$$G_a^{2\times22,22+33} = G_a^{2\times33,22+33} = \sqrt{2}G_a^{22,33} \tag{1}$$

This relationship between the value of G_a for the fundamentals and for their first overtone and combination states is derived from a ratio of harmonic oscillator matrix elements described by equations 17.8.4 and 17.8.6 of Papoušek and Aliev [68]. As progressively higher values of K_a and J were added to the data set, more constants could be satisfactorily

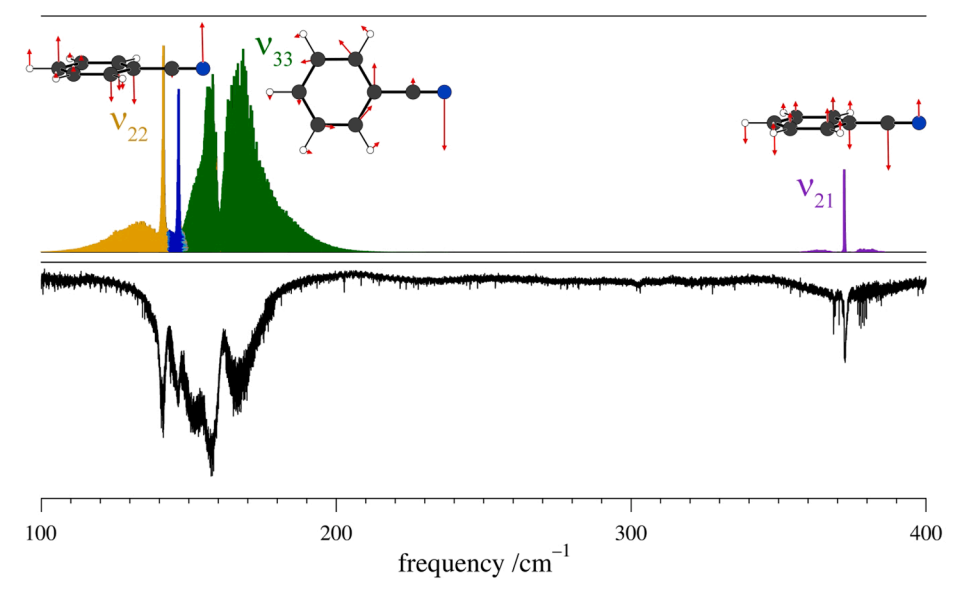


Fig. 5. Benzonitrile infrared spectrum (presented in transmission) from 100 to 400 cm $^{-1}$ (bottom) and stick spectrum of the fundamentals and hot-bands examined in this work (top). Peaks due to residual water have been removed from the experimental spectrum for viewing convenience. Although transitions for the bands between 100 and 200 cm $^{-1}$ are overlapping throughout the frequency range, a region with predominantly $\nu_{22}=1 \leftarrow \text{g.s.}$ is identified in gold, the $\nu_{22}=2 \leftarrow 1$ hot-band is in blue, the $\nu_{33}=1 \leftarrow \text{g.s.}$ band is in green, and $\nu_{21}=1 \leftarrow \text{g.s.}$ is in violet. Images of ring deformations associated with fundamental states are depicted near their labels.

Table 3 Experimentally determined parameters for the ground vibrational state^a; $v_{22} = 1$; $v_{33} = 1$; $v_{22} = 2$; $v_{22} = 1$, $v_{33} = 1$; and $v_{33} = 2$ excited vibrational states^b of benzonitrile. (A-reduced Hamiltonian, I^r Representation).

	g.s. ^a	$v_{22} = 1 \text{ (B}_1, 141 \text{ cm}^{-1}) [20,39]$	$v_{33} = 1 \text{ (B}_2, 163 \text{ cm}^{-1}) [20,39]$	$v_{22} = 2 \text{ (A}_1, 282 \text{ cm}^{-1})^{\text{e}}$	$v_{22} = 1$, $v_{33} = 1$ (A ₂ , 303 cm ⁻¹) ^e	$v_{33} = 2 \text{ (A}_1, 323 \text{ cm}^{-1})^e$
A_{ν} (MHz)	5655.265428 (82)	5654.4 (15)	5654.8 (15)	5653.6498 (20)	5653.7987 (18)	[5654.33463]
B_{ν} (MHz)	1546.8757715 (80)	1548.621345 (48)	1549.726296 (42)	1550.36340 (22)	1551.461223 (45)	1552.54374 (22)
C_{ν} (MHz)	1214.4040832 (69)	1216.238213 (45)	1215.223002 (44)	1218.07069 (23)	1217.040732 (32)	1216.03023 (22)
Δ_J (kHz)	0.0452858 (14)	0.0460141 (30)	0.0461983 (30)	0.0467474 (16)	0.0469414 (14)	0.0471102 (15)
Δ_{JK} (kHz)	0.937983 (20)	0.94764 (35)	0.90712 (35)	0.95532 (22)	0.91750 (14)	0.87582 (26)
Δ_K (kHz)	0.24411 (75)	[0.24411]	[0.24411]	[0.24411]	[0.24411]	[0.24411]
δ_J (kHz)	0.01101116 (54)	0.01108000 (67)	0.01136155 (55)	0.01114909 (73)	0.01142440 (73)	0.01169759 (66)
δ_K (kHz)	0.609187 (65)	0.607270 (91)	0.611417 (81)	0.60709 (11)	0.611127 (92)	0.614320 (82)
Φ_J (Hz)	0.000002486 (60)	0.00000301 (10)	0.00000278 (10)	[0.0000391]	[0.00000371]	[0.00000351]
Φ_{JK} (Hz)	0.0015586 (41)	0.0014080 (19)	0.0016704 (20)	0.0012275 (40)	0.0015695 (74)	0.0017335 (43)
Φ_{KJ} (Hz)	-0.007863 (16)	-0.006060 (95)	-0.009089 (95)	-0.004056 (50)	-0.008793 (83)	-0.009529 (48)
Φ_K (Hz)	[0.0066915]	[0.0066915]	[0.0066915]	[0.0066915]	[0.0066915]	[0.0066915]
ϕ_J (Hz)	0.000001159 (26)	[0.00001159]	[0.00001159]	[0.000001159]	[0.000001159]	[0.000001159]
ϕ_{JK} (Hz)	0.0007398 (24)	0.0007299 (38)	0.0006535 (38)	[0.000743]	[0.000669]	[0.000595]
ϕ_K (Hz)	0.007480 (67)	[0.00748]	[0.00748]	[0.00748]	[0.00748]	[0.00748]
E (MHz)		4241494.43 (17)		8473020.50 (25)		
$E (\text{cm}^{-1})$		141.4810252 (57)		282.6295417 (83)		
ΔE (MHz)			572848.52 (20) ^f		598087.43 (31) ^g	1165078.74 (28) ^g
$\Delta E \text{ (cm}^{-1}\text{)}$			19.1081698 (67) ^f		19.950049 (10) ^g	38.8628436 (93) ^g
G_a (MHz)			9531. (46) ^f	13476.329 (25) ^{h,i}		13476.329 (25) ^{h,i}
G_a^{J} (MHz)			$-0.004594 (20)^{f}$	$-0.007394 (69)^{h}$		$-0.005531 (71)^{h}$
F _{bc} (MHz)			$-0.412(30)^{\text{f}}$	$-0.58568 (16)^{h}$		$-0.58657(14)^{h}$
F_{bc}^{K} (kHz)			$-0.00896 (32)^{f}$	$-0.01106(25)^{h}$		$-0.01124 (20)^{h}$
W (MHz)						$-20649.1 (12)^{g}$
W ^J (MHz)						0.0844 (61) ^g
Δ_i (uÅ ²)	0.0801	-0.1929	0.3932	-0.4632	0.1209	0.7016
$N_{ m lines}^{\ \ j}$	5819	3001 / 2373 ^k	2933 / 6470 ^k	3385 / 1273 ¹	3161 / 0	3152 / 1139 ^l
$\sigma_{\rm fit} ({\rm MHz})^{\rm m}$	0.028	0.035	0.037	0.038	0.053	0.045

^a Constants for ground state from single-state least-squares fit of only rotational data.

b Excited-state constants from six-state least-squares fit including high-resolution infrared and rotational data.

^c Combination and overtone-state constants that could not be determined were held constant at value extrapolated from ground state and corresponding fundamental constants based on single-state ground-state value and corresponding value from the fundamental dyad upon initial incorporation of computational Φ_K value.

^d Δ_K , Φ_K , Φ_I and Φ_K , along with all octic centrifugal distortion constants not listed explicitly, were held constant at the ground-state values from Table 1.

e Predicted frequencies from CCSD(T)/cc-pCVTZ calculation using *xguinea*.

^f ΔE , G_a and F_{bc} parameters are for coupling with the $v_{22} = 1$ vibrational state, which is at lower energy.

^g ΔE and W parameters are for coupling with the $v_{22} = 2$ vibrational state, which is at lower energy.

^h G_a and F_{bc} parameters are for coupling with the $v_{22} = 1$, $v_{33} = 1$ vibrational state.

ⁱ Marked values of G_a fitted to be equal to one another.

^j Number of independent transitions (millimeter-wave / IR).

^k IR transitions from ground to fundamental state.

¹ IR transitions from fundamental to corresponding overtone state.

m Standard deviations for the vibrational state subsets (millimeter-wave): the overall standard deviation of the coupled fit to 5934 lines is 0.039 MHz for millimeter-wave data and 0.00023 cm⁻¹ for IR data.

determined in the least-squares fit. Since the estimates of the energy separations were expected to be more accurate than the estimate of the coupling terms, the values of G_a were allowed to vary in the least-squares fit prior to the energy separations. Inclusion of transitions with even higher quantum number values and transitions whose energy levels were strongly perturbed by coupling required the incorporation of higher-order coupling terms. As a result, both sets of Coriolis coupling terms (for $v_{22} = 2$ to $v_{22} = 1$, $v_{33} = 1$ and for $v_{33} = 2$ to $v_{22} = 1$, $v_{33} = 1$) involve the same terms as the v_{22} - v_{33} dyad: G_a , G_a , F_{bc} , and F_{bc}^K .

Ro-vibrational transitions from the ground vibrational state to $\nu_{22}=1$, to $\nu_{33}=1$, and to $\nu_{21}=1$, as well as hot-band transitions from $\nu_{22}=1$ to $\nu_{22}=2$ and from $\nu_{33}=1$ to $\nu_{33}=2$ were assigned using the

spectroscopic constants acquired as a result of fitting the millimeter-wave data, including coupling terms. The recorded spectra show only partial resolution at the instrument resolution used, as seen in Fig. 5. This data was sufficient, however, to assign numerous transitions to obtain accurate band origins for the fitted states. A strong band that is saturated under the current experimental conditions is additionally visible near 542 cm⁻¹, presumably due to ν_{20} (B₁, 542 cm⁻¹ [20,39]), which is reported to have very strong infrared transitions. A lower-pressure spectrum has been recorded and the investigation of this spectral region will be the subject of a future study.

Although the values of $G_a^{2\times 22,22+33}$ and $G_a^{2\times 33,22+33}$ were different throughout the fitting process of purely rotational data, when the triad

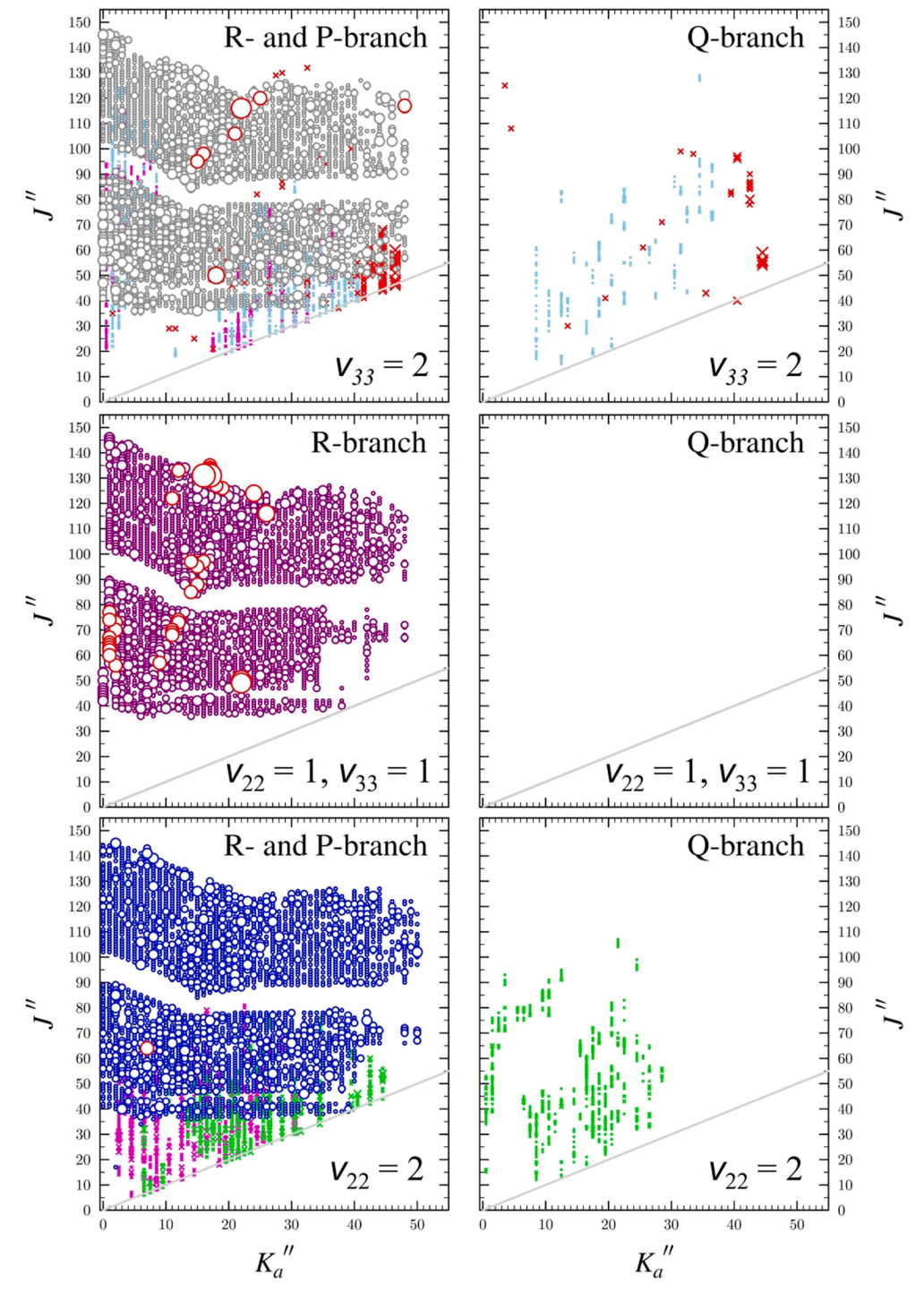


Fig. 6. Data distribution plots for the multistate fit of the first overtones and combination state of ν_{22} and ν_{33} of benzonitrile. The size of the plotted symbol is proportional to the value of $|(f_{\rm obs.} - f_{\rm calc.})/\delta f|$, where δf is frequency measurement uncertainty, and values greater than or equal to 3 are marked in red. Colored circles denote millimeterwave data. Colored crosses mark infrared hot-band data (magenta color denotes P-branch transitions) from the corresponding fundamental to the first overtone, and are shifted up by 0.5 along the K_a axis for viewing convenience.

was combined in a single least-squares fit with the ground state and lower-energy dyad *via* infrared transitions, these two major Coriolis coupling values had to be set equal to one another to achieve a converged least-squares fit and minimize correlations between spectroscopic constants. The least-squares fit of the triad based solely on rotational data is provided in the supplementary material. The constants determined through the six-state data set are provided in Table 3.

Relative to those reported in 2018 [28], the constants of $v_{22}=1$ and $v_{33}=1$ were minimally affected by incorporation into the six-state least-squares fit. As was the case in updating the ground state, Φ_J changed most, changing by approximately 160% ($v_{22}=1$) and 315% ($v_{33}=1$). Such a change is again unsurprising, since the value of Φ_K was updated from a value of zero to being held constant at the value predicted for the ground vibrational state. This change in the sextic constant affects, in particular, the other sextic and higher-order constants. The other sextic constants changed by less than 3%. The octic constants for both fundamentals are held at the corresponding ground-state values. The quartic and rotational constants changed by less than 0.2%.

Data distribution plots for the triad states are provided in Fig. 6. The lower intensity relative to the $\nu_{22}=1$ and $\nu_{33}=1$ fundamentals results in fewer measurable transitions for the higher-energy triad states. The

number of measured transitions for the triad states reported here is nearly the same as for the lower-energy dyad states due to the fact that the triad incorporates transitions from the new 130-230 GHz frequency range, while the dyad does not. This data was sufficient to analyze the Coriolis and Darling-Dennison couplings. There are several high-error transitions in the millimeter-wave data of $v_{22} = 1$, $v_{33} = 1$ and in the infrared data of $v_{33} = 2$. The millimeter-wave data depicted in Fig. 6 is the same data that was included in the purely millimeter-wave leastsquares fit of the triad. Nearly all of these data points were well-fit in the isolated triad data set. In addition to those depicted in Fig. 6, just over 30 infrared transitions were initially assigned to the $v_{33} = 1$ to $v_{33} = 2$ hotband that were excluded from the six-state least-squares fit (provided in the supplementary materials) due to high obs. - calc. values. The infrared transitions that show high error in Fig. 6 and the excluded transitions also appeared with lower error when using the rotationally determined spectroscopic constants to predict the infrared frequencies, and their assignments are reasonable based on combination differences analysis. It is therefore somewhat unclear why these transitions are not well fit when combined into the six-state least-squares fit. It is possible that, in combining the ground vibrational state, lowest-energy fundamental dyad, and corresponding first overtone and combination state triad into

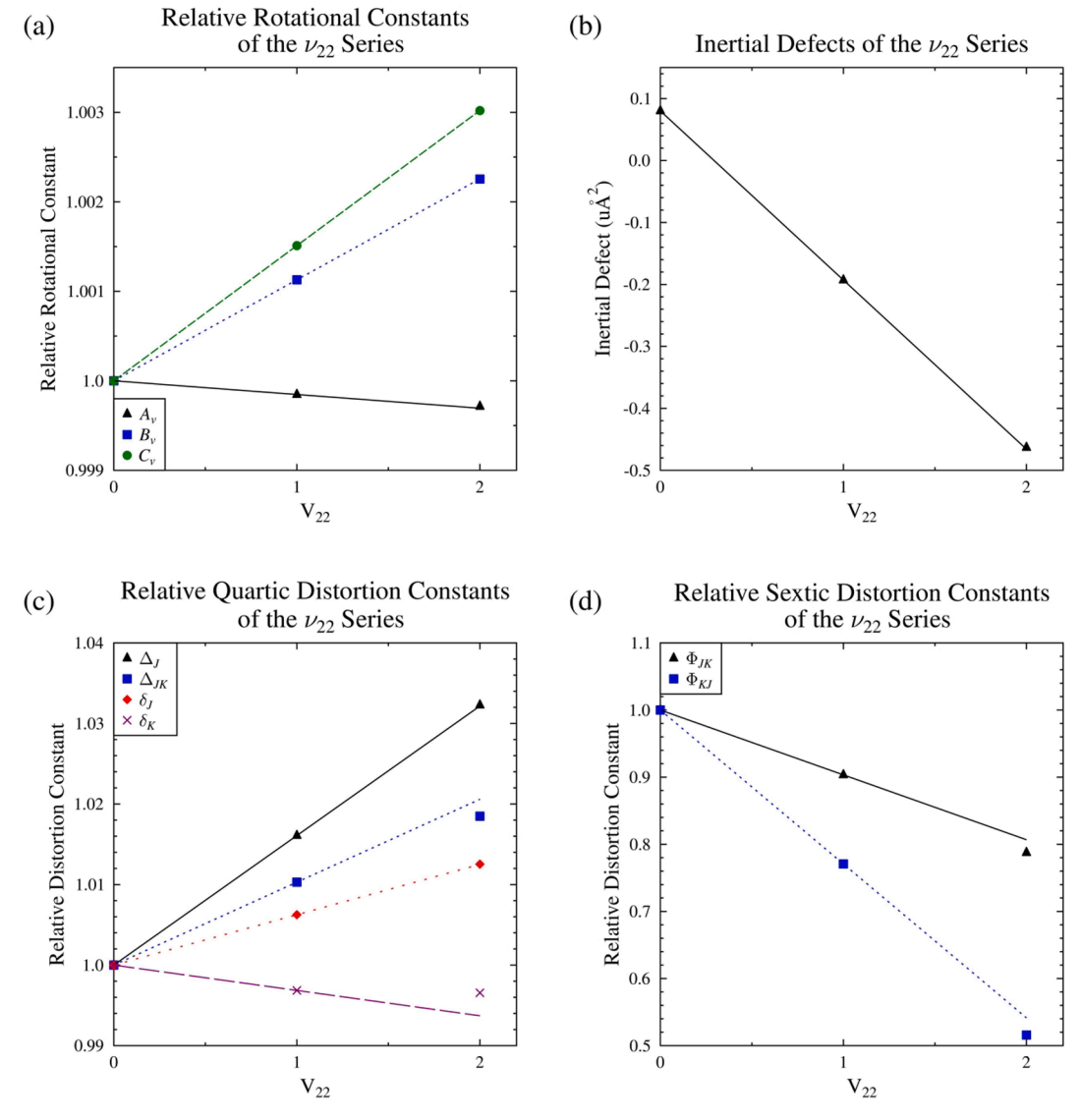


Fig. 7. (a) Rotational constants relative to ground-state values, (b) inertial defect, (c) fitted quartic centrifugal distortion constants relative to ground-state values, and (d) fitted sextic centrifugal distortion constants relative to ground-state values of the v_{22} series as a function of vibrational quantum number. Lines show values extrapolated from the experimental ground state and $v_{22} = 1$ values, while symbols represent experimental values.

a single, six-state least-squares fit, the correlations between numerous spectroscopic constants and the need to hold many constants at predicted values introduce additional error into the fitting compared to isolated least-squares fits. Alternately, given the pattern of many higherror transitions occurring at high quantum-number values (and those that were excluded having even higher ones, just at or above the K_a values included in the millimeter-wave data), it is possible these transitions exhibit unaddressed coupling that would require higher-order terms to fit, but there is still insufficient data to determine those constants. An observation that affords some credence to this possibility is that fitting of the excluded infrared transitions resulted in the values of A_{ν} and Δ_{K} for $\nu_{22}=1$ and $\nu_{33}=1$ diverging substantially from the corresponding ground-state values by approximately equal and opposite magnitudes - a hallmark of the a-type Coriolis perturbation being absorbed into the rotational and distortion constants. To prevent this artificial distortion of the spectroscopic constants, those transitions that could not be fit with spectroscopic constants that appear physically meaningful were excluded. Despite the remaining high-error transitions and somewhat larger than desirable σ of $v_{22} = 1$, $v_{33} = 1$, the quality of the spectroscopic constants determined in the multi-state fit is expected to be good based on the analyses described below.

If coupling is treated properly, the change in rotational and

centrifugal distortion constants from ground vibrational state to increasing quanta of the fundamental states should be approximately linear. Figs. 7 and 8 show the ratio of the v_{22} and v_{33} series, respectively, rotational constants (Fig. 7a and 8a), quartic centrifugal distortion constants (Fig. 7c and 8c), and sextic centrifugal distortion constants (Fig. 7d and 8d) relative to those of the ground state, as well as the inertial defect trends (Fig. 7b and 8b), as a function of vibrational quantum number. As shown in Table 3 and represented graphically in Figs. 7 and 8, the changes in the rotational constants and inertial defect are essentially indistinguishable from their extrapolated values (with the exception of $A_{2\times33}$, which could not be determined due to the availability of only a-type transitions and the correlations between the A_{ν} constants, purely K-dependent parameters, and Coriolis-coupling terms). The quartic distortion constants are quite well-behaved, differing by less than 0.3% from their extrapolated values. While the sextic constants visually appear to differ drastically from their extrapolated values, even these values are within 8% of the extrapolated values - a quite reasonable level of agreement for the sextic distortion constants. By an analogous analysis, the spectroscopic constants for $v_{22} = 1$, $v_{33} = 1$ presented in Table 3 are very near to their extrapolated values. The rotational constants differ from their extrapolated values by less than 0.01%, and the quartic distortion constants are within 0.3%. The value of Φ_{KI} shows

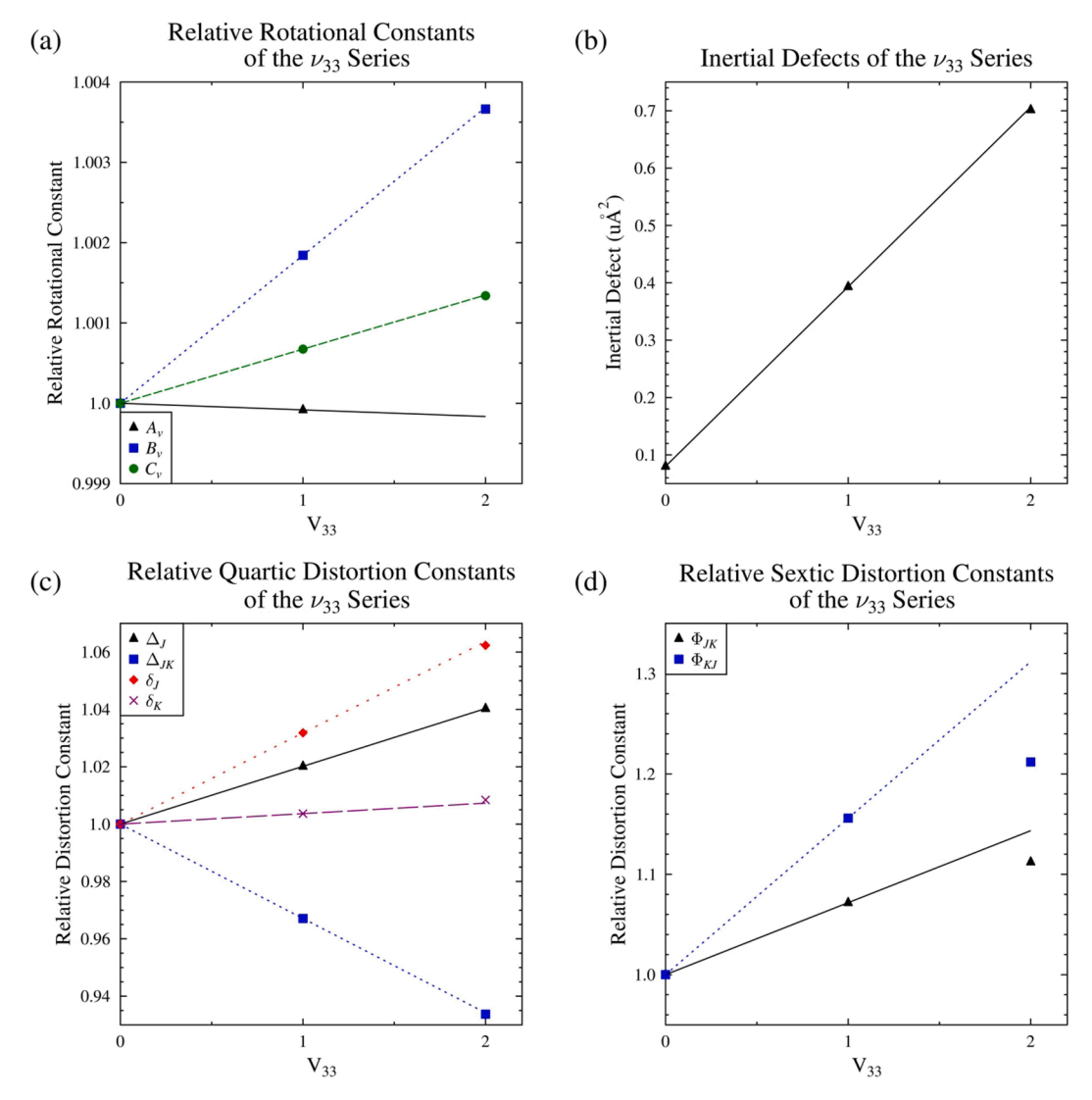


Fig. 8. (a) Rotational constants relative to ground-state values, (b) inertial defect, (c) fitted quartic centrifugal distortion constants relative to ground-state values, and (d) fitted sextic centrifugal distortion constants relative to ground-state values of the ν_{33} series as a function of vibrational quantum number. Lines show values extrapolated from the experimental ground state and $\nu_{33}=1$ values, while symbols represent experimental values.

a larger discrepancy from the extrapolation, differing by 21%. While this difference may indicate some error in the coupling analysis, the value of Φ_{KJ} is still between the overtone values and appears to be reasonable. Overall, we believe that we were successfully able to minimize the amount of perturbation absorbed into the rotational and centrifugal distortion constants, and that these constants can be reasonably expected to be close to physically meaningful values.

4.2.1. Analysis of coupling interactions in the triad

The $v_{22} = 2$; $v_{22} = 1$, $v_{33} = 1$; and $v_{33} = 2$ triad provides the opportunity to examine an interplay of Coriolis and Darling-Dennison coupling. The spectra of all three excited states have hallmarks of these interactions, but the lower-energy Coriolis-coupled dyad ($v_{22} = 2$ to $\nu_{22}=1,\,\nu_{33}=1)$ and higher-energy Coriolis-coupled dyad ($\nu_{22}=1,$ $v_{33}=1$ to $v_{33}=2$) are not equivalent in appearance. Fig. 9 shows resonance plots of the $K_a = 9^J$ series for the three excited states, highlighting the global undulation of each. (Superscripts J and J+1 on values of K_a indicate the energy-level symmetries in the corresponding ^aR_{0.1} transitions [69].) These undulations are largely due to the interaction of the Darling-Dennison resonance and the Coriolis perturbation $(\Delta K_a = 0)$ with a change in behavior from oblate to prolate in the asymmetric rotor problem as *J* increases [32]. The lowest- and highestenergy vibrational states of the triad display more drastic curvature with inverted peak and trough, quite similar in shape to, though with larger amplitude than, those observed in the corresponding fundamental states. The combination state, as expected, exhibits an intermediate curvature.

Another set of resonance plots is presented in Fig. 10, highlighting local resonances due to the a-type Coriolis interactions in the two dyads. In accordance with a-type Coriolis selection rules, resonant interactions occur between opposite-symmetry states with even values of ΔK_a . While the lower J''+1 end of the $v_{22}=2$ series depicted is non-degenerate, the $K_a=12^{J+1}$ series is degenerate with $K_a=11^J$ in the J''+1 range of the resonance. The $K_a=8^J$ series of $v_{22}=1$, $v_{33}=1$ in the depicted range is degenerate with the $K_a=9^{J+1}$ series. Therefore, the v_{22} overtone and combination band have degenerate $\Delta K_a=2$ and $\Delta K_a=4$ interactions at J''+1=115. The resulting transition frequency displacement is relatively small. The same $v_{22}=1$, $v_{33}=1$ K_a series are resonant with $v_{33}=2$ (degenerate $K_a=5^J$, 6^{J+1}) by $\Delta K_a=2$, 4 selection rules at J''+1=99 and 100, resulting in a much larger transition frequency displacement (~400 MHz from the unperturbed frequency at J''+1=100). The

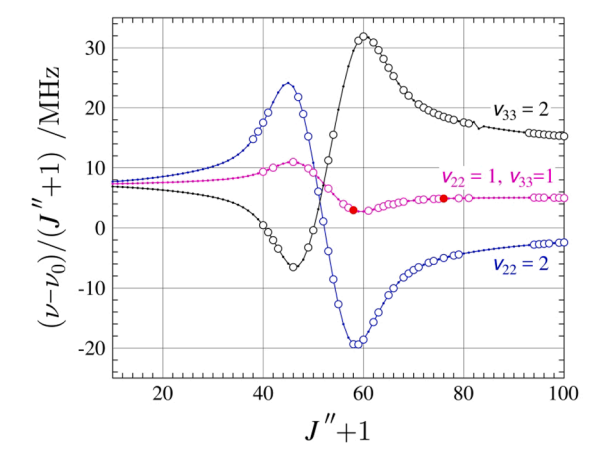


Fig. 9. Difference frequency plot for $K_a=9^J$ rotational transition sequences in $\nu_{22}=2$ (blue), $\nu_{22}=1$, $\nu_{33}=1$ (magenta) and $\nu_{33}=2$ (black) vibrational states, indicating the effect of distortion and perturbation among the three states. The plotted values are frequency differences between excited state transitions and their ground-state counterparts, scaled by (J''+1) in order to make the plots more horizontal. Measured transitions are represented by open circles, while red circles indicate measurements with $|(f_{\rm obs.}-f_{\rm calc.})/\delta f|\geq 3$. A resonance is visible near J''+1=84 for $\nu_{33}=2$.

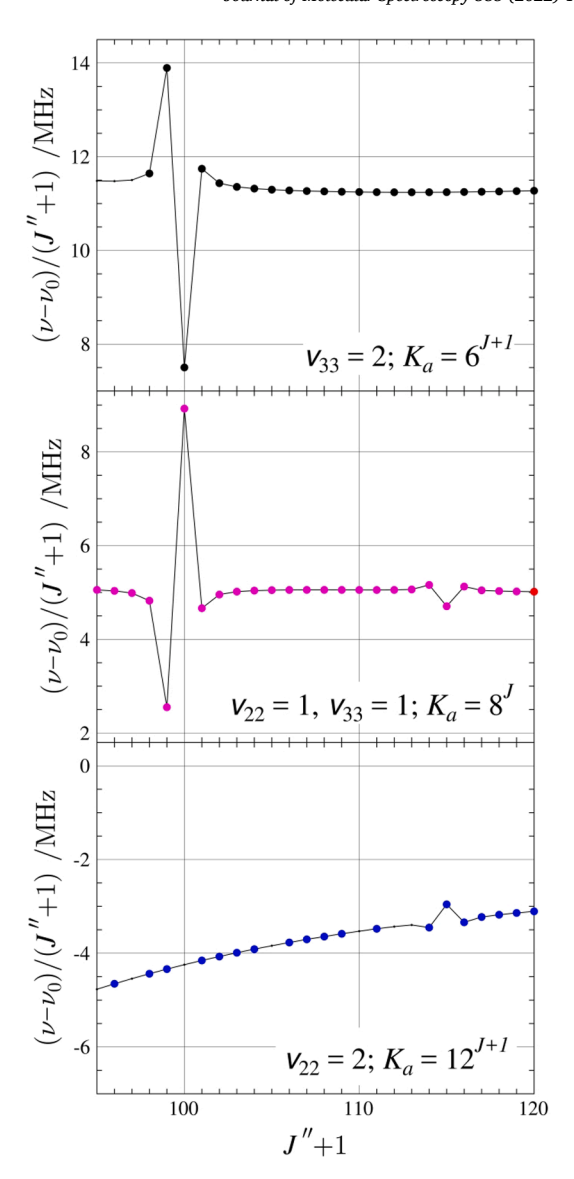


Fig. 10. Resonance plots depicting degenerate $\Delta K_a=2$ and $\Delta K_a=4$ local perturbations between $\nu_{22}=2$ and $\nu_{22}=1$, $\nu_{33}=1$ at J''+1=115 and between $\nu_{22}=1$, $\nu_{33}=1$ and $\nu_{33}=2$ at J''+1=99, 100. At J''+1=115, the $\nu_{22}=2$ $K_a=12^{J+1}$ series is degenerate with $K_a=11^J$. In the depicted J''+1 range, the $\nu_{22}=1$, $\nu_{33}=1$ series is degenerate $K_a=8^J$, 9^{J+1} , and the $\nu_{33}=2$ series is degenerate $K_a=5^J$, 6^{J+1} . Measured transitions are represented by circles and predictions from the final coupled fit are black lines. Red circles indicate transitions with $|(f_{\rm obs.}-f_{\rm calc.})/\delta f|\geq 3$. The three plots have identical scaling along the vertical axis, and the respective exact mirror image correspondence confirms the K_a assignment of the resonance partners.

resonances shown here are fairly representative for the respective pairs of states – resonances between $v_{22}=2$ and $v_{22}=1$, $v_{33}=1$ tend to be quite a bit smaller than those between $v_{33}=2$ and $v_{22}=1$, $v_{33}=1$. While it is difficult to pinpoint the origin of this asymmetry in behavior, it is clear that the two sets of dyads are not symmetric in their perturbation behaviors. Because the Coriolis perturbation parameters and the vibrational energy separations of these two pairs of interacting states are very similar, the gross asymmetry observed is somewhat surprising. It is certainly true that the changes in the W parameter cause noticeable changes in the V and V0 positions and the amplitudes of the frequency shifts in the resonances. This, in fact, is one of the reasons that the V1 parameter can be determined from the rotational spectrum as well as it can be. It also assists in mitigating the statistical correlation between V2 and the energy separations obtained from the successful multi-state

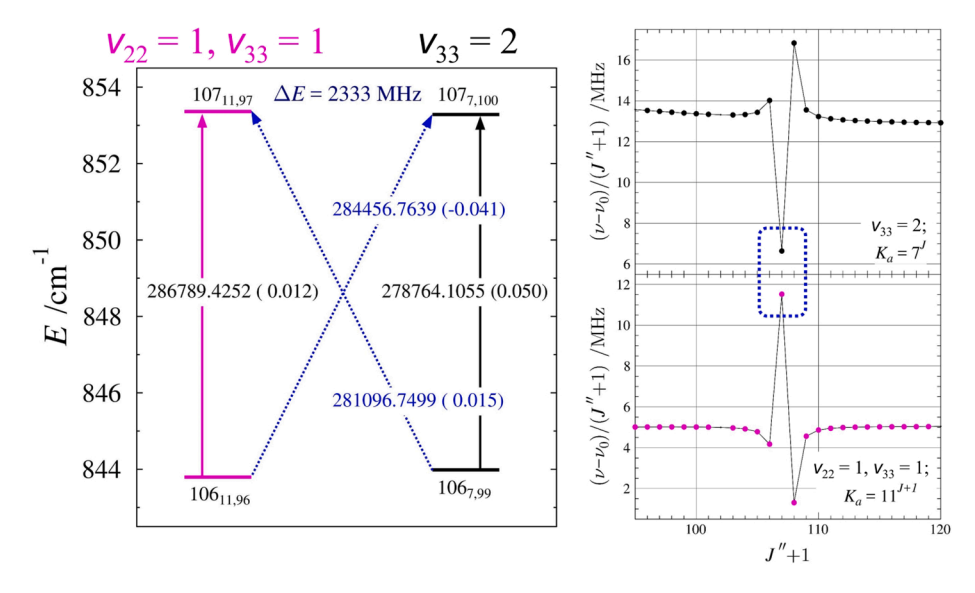


Fig. 11. Energy diagram illustrating the origin of representative nominal rotation-vibration transitions between $\nu_{22}=1$, $\nu_{33}=1$ and $\nu_{33}=2$ vibrational states alongside resonance plots featuring the corresponding, highly displaced within-state transitions (highlighted in dashed, blue rectangle). The vertical arrows mark the standard $^aR_{0,1}$ pure rotational transitions, while the slanted arrows indicate the transitions enabled by strong mixing between rotational levels in the two vibrational states. The marked transition frequencies are in MHz and the quantities in parentheses are obs.-calc. values from the final fit. The ΔE value in navy is the energy difference between the closest levels.

regression analysis including infrared data, as is the assumption that the two G_a values are equivalent. A notable and important point for the discussion of harmonic frequencies (ω_i) and anharmonicity terms (x_{ij}) that follows is that, because the Darling-Dennison perturbation parameter W is treated explicitly in our multi-state least-squares fit, the term energies determined from that fit and employed below are already deperturbed with respect to effects of the Darling-Dennison perturbation.

The apparently stronger interaction between $v_{33} = 2$ and $v_{22} = 1$, v_{33} = 1 makes it unsurprising that we were able to assign nominal interstate transitions only for this dyad and none for the lower-energy dyad. Once the coupling is well-modeled by the least-squares fit, it becomes practical to look for such formally forbidden transitions, which are enabled by the quantum mixing between states. For the v_{33} overtone and combination band, we identified seven matched pairs of nominal interstate transitions. An example of such a set of transitions, along with their corresponding within-state transitions is shown in Fig. 11. As highlighted in the resonance plots, the within-state transition frequencies are strongly displaced as a result of the interaction between vibrational states. Also due to this relatively strong state mixing, the nominal interstate transitions are afforded intensity from the within-state transitions and become observable. In the given example, the upper rotational energy levels are closest together, separated by 2333 MHz. The nominal interstate assignment is confirmed by the fact that the difference between the average frequency of the interstate transitions and the average of the within-state transition frequencies - a value that should be equal to zero - is 8 kHz, well within the 50 kHz measurement uncertainty.

4.3. Higher-energy fundamentals ν_{21} and ν_{15}

The third lowest-energy fundamental, $\nu_{21}=1$ (B₁, 372 cm⁻¹), is a butterfly motion of the ring where the H and C atoms lying on the a-axis (including the nitrile C atom) move out of plane in one direction, and the other atoms move in the opposite direction. Approximately 20 cm⁻¹ higher in energy is $\nu_{15}=1$ (A₂, 397 cm⁻¹), where all atoms lying on the a-axis remain stationary, while the off-axis C and H atoms of the ring move out of plane such that atoms diagonal to one another move in the same direction, but opposite the direction of the other set of moving atoms. Both of these fundamentals were predicted and initially least-squares fit using single-state, distorted-rotor models from the experimental ground-state constants and computed $B_0 - B_{\nu}$ values. The spectroscopic constants determined using the millimeter-wave data for $\nu_{21}=1$ were subsequently used to predict and incorporate infrared data into its least-squares fit. The $\nu_{15}=1$ state is not infrared active. As $\nu_{21}=1$ and

 $v_{15} = 1$ are predicted to have an energy separation similar to the abovedescribed interacting vibrational states, and their intensities are only slightly lower than those of the triad states (resulting in a very similar range of observable J and K_a values), it is unsurprising that observed transitions for $v_{21} = 1$ and $v_{15} = 1$ exhibit coupling in the *J* and K_a values accessible in our spectral data. The first clear indication of a resonance appears near J''=95 at $K_a=12$ for $v_{21}=1$ and $K_a=10$ for $v_{15}=1$. These fundamentals are c-type Coriolis-coupled, but lack a first-order $\zeta^c_{21.15}$ contribution to G_c , due to the equation giving $\zeta^c_{21,15}$ involving a summation over terms that are all equal to zero for two out-of-plane vibrations. For both $v_{21}=1$ and $v_{15}=1$, millimeter-wave transitions with values of $K_a = 0$ to 40 were included in the data presented here. For v_{21} = 1, the presently reported millimeter data includes J'' values from 36 to 147, while this range is from 36 to 142 for $v_{15} = 1$. Additionally, 1072 transitions from the ground state to $v_{21} = 1$ were measured in the infrared data, ranging in J'' from 7 to 114 and in K_a from 0 to 44. The breadth of data for $v_{21}=1$ and $v_{15}=1$ is depicted in Fig. 12. Each data distribution plot contains a couple of evident gaps that are not due to gaps in frequency coverage. Beginning near the aforementioned J'' = 95and $K_a = 12$ for $v_{21} = 1$ and $K_a = 10$ for $v_{15} = 1$, there is a diagonal region of missing transitions that moves to higher J'' and K_a , as it expands in width. This gap is due to the exclusion of transitions that are near local resonances. As demonstrated in previous works [10,11,29,30,32], resonances tend to increase in magnitude as they move to higher quantumnumber values. As a result, more transitions are excluded near these regions at higher J'' and K_a . Another gap for both of these states appears in the upper-right quadrant of the data distribution plots. While many of these transitions were assignable, we excluded them to eliminate at least some of the perturbation experienced by the interacting states. Additionally, $v_{15} = 1$ is expected to be approximately 26 cm⁻¹ lower in energy than $v_{22} = 3$, which may add further complexity to the rotational spectrum of the former. We have begun a coupled-state analysis for v_{21} = 1 and v_{15} = 1, but, due the complexity of such a least-squares fit, provide here preliminary spectroscopic constants for each fundamental based on single-state models (Table 4).

Though the spectroscopic constants for $v_{21}=1$ and $v_{15}=1$ reported in Table 4 are almost certainly being distorted by absorbing some of the Coriolis interaction between the fundamentals, we expect that these constants are reasonably close to their true physical values. The rotational constants of either fundamental vary from the corresponding ground-state values by less than 0.2%. The value of Δ_K shows the largest discrepancy from the ground-state value for both $v_{21}=1$ and $v_{15}=1$ (13% and 6%, respectively). The other quartic centrifugal distortion constants are all within 1% of the corresponding ground-state values. Of

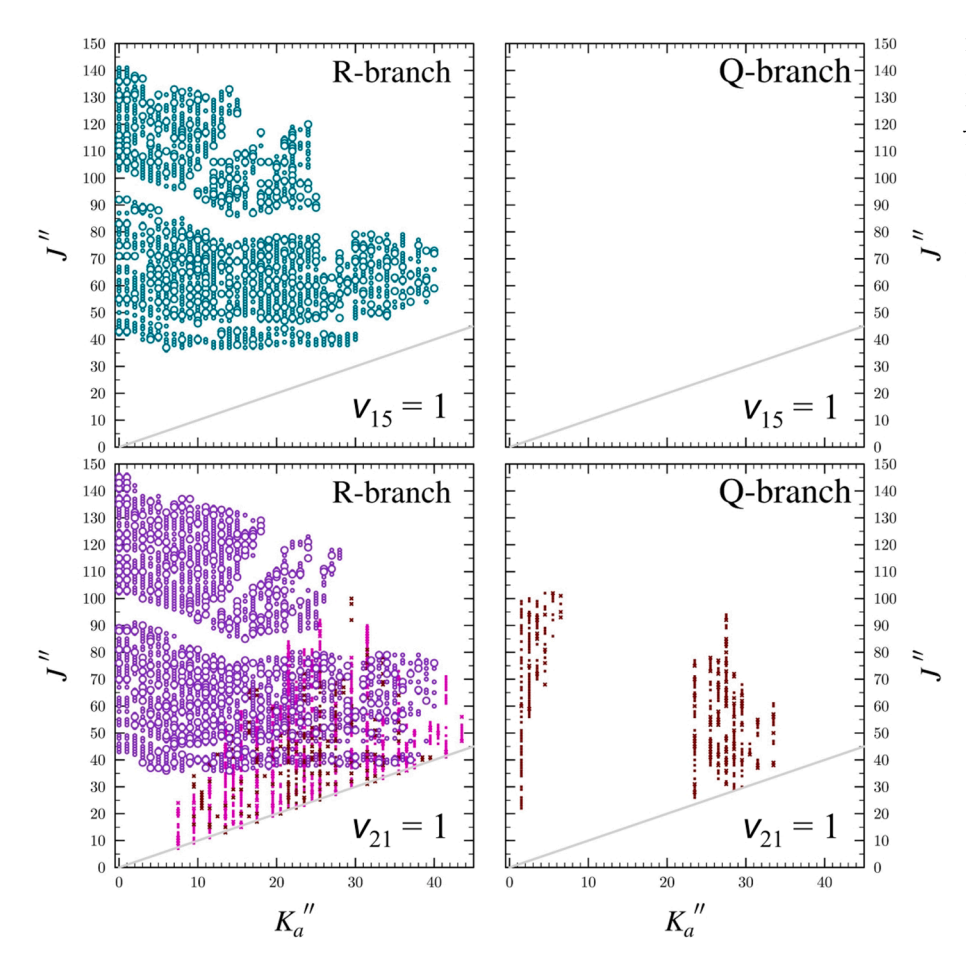


Fig. 12. Data distribution plots for $\nu_{21}=1$ (bottom) and $\nu_{15}=1$ (top) of benzonitrile. The size of the plotted symbol is proportional to the value of $|(f_{\rm obs.}-f_{\rm calc.})/\delta f|$, where δf is frequency measurement uncertainty, and all values are smaller than 3. Circles denote millimeter-wave data. Colored crosses mark infrared data from the ground vibrational state to $\nu_{21}=1$ (magenta color indicates P-branch transitions), and are shifted up by 0.5 along the K_a axis for viewing convenience. The ν_{15} mode is not infrared active.

Table 4 Experimentally determined parameters for the ground vibrational state, $v_{21} = 1$, and $v_{15} = 1$ of benzonitrile. (A-reduced Hamiltonian, I^r Representation). ^{a,b}

	g.s.	$v_{21} = 1^{\circ} (B_1, 372 \text{ cm}^{-1}) [20,39]$	$v_{15} = 1 \text{ (A}_2, 397 \text{ cm}^{-1}) [20,39]^d$
A_{ν} (MHz)	5655.265428 (82)	5643.72210 (91)	5649.8980 (24)
B_{ν} (MHz)	1546.8757715 (80)	1547.385653 (70)	1547.145494 (69)
C_{ν} (MHz)	1214.4040832 (69)	1215.350223 (48)	1215.109219 (65)
Δ_J (kHz)	0.0452858 (14)	0.0454438 (50)	0.0454588 (55)
Δ_{JK} (kHz)	0.937983 (20)	0.937772 (94)	0.93422 (12)
Δ_K (kHz)	0.24411 (75)	0.21365 (60)	0.2301 (31)
δ_J (kHz)	0.01101116 (54)	0.0110407 (31)	0.0110260 (12)
δ_K (kHz)	0.609187 (65)	0.60344 (15)	0.60877 (26)
Φ_J (Hz)	0.000002486 (60)	0.00000306 (21)	0.00000459 (19)
Φ_{JK} (Hz)	0.0015586 (41)	0.0016063 (48)	0.0015664 (81)
Φ_{KJ} (Hz)	-0.007863 (16)	-0.008313 (65)	-0.007287 (75)
Φ_K (Hz)	[0.0066915]	[0.0066915]	[0.0066915]
ϕ_J (Hz)	0.000001159 (26)	0.00000163 (12)	[0.00001159]
ϕ_{JK} (Hz)	0.0007398 (24)	0.0008529 (65)	0.0007564 (97)
ϕ_K (Hz)	0.007480 (67)	[0.007480]	[0.007480]
E (MHz)		11160013.88 (31)	[11901760.6]
$E \text{ (cm}^{-1}\text{)}$		372.257993 (10)	[397]
Δ_i (uÅ ²)	0.080081 (3)	-0.319017 (26)	-0.189355 (46)
$N_{\rm lines}^{\rm e}$	5819	1992 / 1072 ^f	1642
$\sigma_{\rm fit}$ (MHz)	0.028	$0.041 / 0.0002^{g}$	0.042

^a Φ_K held constant at the value predicted for the ground vibrational state.

 $^{^{\}mathrm{b}}$ ϕ_{K} , along with all octic centrifugal distortion constants not listed explicitly, fixed at the ground-state values from Table 1.

^c Values shown in table based on combined fit of millimeter-wave and infrared data.

 $^{^{\}rm d}$ Vibrational frequency measured \emph{via} Raman spectroscopy.

^e Number of independent transitions.

 $^{^{\}rm f}$ Millimeter-wave transitions / ground state to $\nu_{21}=1$ IR transitions.

 $^{^{\}rm g}\,$ RMS error for millimeter-wave data / IR data.

Table 5 Experimental and computed vibration–rotation interaction constants (α_i values) for $\nu_{21}=1$ and $\nu_{15}=1$ excited vibrational states of benzonitrile.

	$v_{21}=1$	$v_{15}=1$	Mean ^a
Expt. perturbed			
$A_{\nu}-A_0$ (MHz)	-11.54333 (91)	-5.3674 (24)	-8.4554 (13)
$B_{\nu}-B_0$ (MHz)	0.509882 (70)	0.269723 (69)	0.389802 (50)
$C_{\nu}-C_0$ (MHz)	0.946140 (48)	0.705136 (65)	0.825638 (41)
Calc. CCSD(T)/AN	101		
$A_{\nu}-A_0$ (MHz)	-11.8	-5.42	-8.62
$B_{\nu}-B_0$ (MHz)	0.474	0.279	0.377
$C_v - C_0$ (MHz)	0.915	0.700	0.807

^a The average of values for the two states, equal to $[(A_{21} - A_0) + (A_{15} - A_0)]/2$, for example.

the sextic constants, Φ_J shows the largest change from ground-state to $\nu_{15}=1$ (85%), while ϕ_J shows the largest difference for $\nu_{21}=1$ (41%). Such small changes from the ground to the excited states could reasonably be expected even without coupling, so we expect that perturbation has not drastically distorted the spectroscopic constants for either fundamental. Since the frequency of $\nu_{21}=1$ has been determined ν ia infrared spectroscopy, analysis of the Coriolis coupling between $\nu_{21}=1$ and $\nu_{15}=1$ would allow determination of the two fundamental states' energy separation, and therefore the energy of the infrared-inactive ν_{15} .

4.4. Comparison of experiment to prediction

The current work provides an opportunity to compare experimentally determined spectroscopic parameters with those predicted by computation at the CCSD(T)/ANO1 level of theory. Table 5 provides a comparison of the vibration–rotation interaction constants for $\nu_{21}=1$ and $\nu_{15}=1$. The agreement between theory and experiment is highly satisfying. The largest discrepancy (in the value of $A_{21}-A_0$) is less than 0.3 MHz, and the other predicted vibration–rotation interaction constants vary from experiment by less than 0.06 MHz.

A combination of experimental and computational data were used to predict the coupling terms in the triad of interest to the present work. Table 6 shows the comparisons between the predicted and determined coupling values. The updated CCSD(T)/ANO1 value of G_a (9408 MHz) for the Coriolis coupling between $v_{22} = 1$ and $v_{33} = 1$ is in good agreement with the experimentally determined value (9531 (46) MHz),

differing by less than 1.3%. As described above, the predicted value of G_q for each of the corresponding first overtone-combination state, Coriolis-coupled dyads was based on the experimental value of G_a for $v_{22} = 1$ and $v_{33} = 1$. Although the values of G_a for the two dyads were held equal to one another in the multi-state fit, this fitted value differs from the estimated one by only 0.02%. Whether or not the same factor of $\sqrt{2}$ would necessarily apply to the higher-order coupling terms, i.e. G_a^J , F_{bc} , and F_{bc}^{K} , was not known to us a priori, since the corresponding equations were not available. After completion of the fitting process, however, it was noted that these constants seemed to scale in a similar way. Empirically, we found that the same scaling factor is preserved to a high degree. The value of G_a^J is smaller than the value scaled in this way by 12.1% for the lower-energy dvad and 17.5% larger than the scaled value for the higher-energy dyad. The average of these two values is only 0.5% from the scaled value. This is reminiscent of the pattern observed during triad fitting, when the two values of G_a were allowed to differ – one value was somewhat larger than predicted, and one somewhat smaller, but their average was very close to the estimated value. Both determined values of F_{bc} are within 0.7% of the predicted value. The values of F_{bc}^{K} are larger than the predicted value by 12.7% and 14.6% in the lower- and higher-energy dyads, respectively. Overall, however, each set of Coriolis-coupling terms appears to be scaled relative to the dyad of the corresponding fundamental states by the approximate factor of $\sqrt{2}$.

The Darling-Dennison interaction term required computational prediction (Table 6). A Darling-Dennison interaction is a type of anharmonic interaction, as is a Fermi interaction. Unlike the Fermi interaction, where the change in vibrational quantum number differs by three, a Darling-Dennison interaction is defined by a change in vibrational quantum number of two or four (in this particular case: four). Such an interaction was originally studied in the water molecule in 1940 [70]. Stanton and coauthors were able to estimate the stretching-level energies of water with great success and provided corrected perturbation theory expressions for several types of vibrational quantum-number changes [71]. As used in the initial estimate of the W in this work, the value of the Darling-Dennison interaction term is indeed related to one eighth of the corresponding quartic force constant ($\frac{\phi_{22,22,33,33}}{8} = 7.92 \text{ cm}^{-1}$, CCSD(T)/ANO1). There are, however, kinetic energy and cubic force constant contributions [71] that should not be ignored for an accurate estimate (Eq. (2)).

$$W = \frac{1}{2}K_{22,22,33,33} = \frac{1}{8}\phi_{22,22,33,33} - \frac{1}{2}\sum_{\alpha}B_{\alpha}^{e}\left(\zeta_{22,33}^{\alpha}\right)^{2}\frac{(\omega_{22}+\omega_{33})^{2}}{\omega_{22}\omega_{33}} + \frac{1}{2}\sum_{k}\frac{1}{8}\phi_{k,22,22}\phi_{k,33,33}\omega_{k}\left[\frac{1}{4\omega_{22}^{2}-\omega_{k}^{2}} + \frac{1}{4\omega_{33}^{2}-\omega_{k}^{2}}\right] - \frac{1}{2}\sum_{k}\frac{1}{2}\phi_{k,22,33}^{2}\frac{\omega_{k}}{\omega_{k}^{2}-(\omega_{22}-\omega_{33})^{2}}$$
(2)

Table 6 Experimental and scaled Coriolis-coupling terms for the interaction of $v_{22}=2$ and $v_{33}=2$ with $v_{22}=1$, $v_{33}=1$; experimental and computed Darling-Dennison interaction terms, of benzonitrile.

	Coriolis				
	Scaled value ^a	$v_{22} = 2$ with $v_{22} = 1$, $v_{33} = 1$	$v_{33}=2$ with $v_{22}=1,v_{33}=1$	Expt. average ^b	
G _a (MHz)	13478.869	13476.329 (25) ^c	13476.329 (25) ^c	13476.329 ^c	
G_a^{J} (MHz)	-0.00650	-0.007394 (69)	-0.005531 (71)	-0.00646	
F_{bc} (MHz)	-0.5827	-0.58568 (16)	-0.58657 (14)	-0.5861	
F_{bc}^{K} (kHz)	-0.0127	-0.01106 (25)	-0.01124 (20)	-0.0112	
		Darling-Dennison,	$v_{22} = 2 \text{ with } v_{33} = 2$		
	Calc.d	Expt.			

^a Value predicted based on corresponding interaction term from $v_{22} = 1 / v_{33} = 1$ dyad multiplied by $\sqrt{2}$.

-0.688780(40)

-0.7017

b Average of corresponding interaction constant values from $\nu_{22}=2$ with $\nu_{22}=1$, $\nu_{33}=1$ pair and $\nu_{33}=2$ with $\nu_{22}=1$, $\nu_{33}=1$ pair.

^c Values of G_a held equal to one another.

^d Evaluated at CCSD(T)/ANO1 using thexguinea module of CFOUR.

Table 7 Experimental and predicted anharmonicity constants related to the ν_{22} and ν_{33} states of benzonitrile.

	Calc. ^a	Expt.
$x_{22,22} \text{ (cm}^{-1}\text{)}$	-0.1702	-0.1663
$x_{33,33} \text{ (cm}^{-1}\text{)}$	0.1324	0.1570
$x_{22,33} \text{ (cm}^{-1})$	0.5099	0.4909

^a Evaluated at CCSD(T)/ANO1.

Table 8 Experimental and computed term energies of six lowest-energy vibrationally excited states of benzonitrile and semi-experimental and computed harmonic frequencies of the ν_{22} and ν_{33} fundamentals.

Anharmonic Term Energie	s (cm ⁻¹)	
	Calc. ^a	Expt. ^b
$v_{22} = 1$	141.40	141.4810252 (57)
$v_{33} = 1$	161.28	160.5891953 (47)
$v_{22}=2$	282.47°	282.6295417 (83)
$v_{22} = 1, v_{33} = 1$	303.11	302.5795909 (87)
$v_{33}=2$	322.66 ^c	321.4923856 (77)
$v_{21}=1$	371.32	372.257993 (10)
Harmonic Frequencies (cm	n ⁻¹)	
	Calc. ^a	Semi-Expt.
ω_{22}	142.93	142.9991
ω_{33}	161.76	161.0147

^a Evaluated at CCSD(T)/ANO1.

Fortunately, the value of W resulting from Eq. (2) is conveniently calculated by the *xguinea* module of CFOUR. As is evident from the computational value of -0.7017 in Table 6, the kinetic energy and cubic force constant terms outweigh the quartic force constant term, resulting in a negative and much smaller net value of W. The final agreement between computation and experiment obtained for benzonitrile is remarkable - a discrepancy of only 2% in the value of W. The method (Eq. (2) evaluated at the CCSD(T)/ANO1 level of theory) used to estimate this value (and the term energies, *vide infra*) therefore appears to be accurate, not only for water, but even for a somewhat larger organic molecule like benzonitrile.

The infrared analysis included in the current work enabled the determination of absolute vibrational energies (deperturbed with respect to W, $vide\ supra$), and the determination of such energies for all states in the $v_{22}=1$; $v_{33}=1$ dyad and corresponding overtone and combination state triad enabled the experimental estimation of the corresponding anharmonicity constants: $x_{22,22}$, $x_{33,33}$, and $x_{22,33}$. The anharmonicity constants, harmonic frequencies (ω), and energies (ω) are related [68] through Eq. (3):

$$E_{v,v,v...} = \sum_{i=1}^{3N-6} \left(v_i + \frac{1}{2}\right) \omega_i + \sum_{i}^{3N-6} \sum_{i \ge i}^{3N-6} \left(v_i + \frac{1}{2}\right) \left(v_j + \frac{1}{2}\right) x_{ij}$$
 (3)

By solving for the energy separation between the ground vibrational state and a fundamental state, one obtains Eq. (4):

$$\nu_i \equiv \Delta E_{0,i} = \omega_i + 2x_{i,i} + \frac{1}{2} \sum_{i \neq i}^{3N-6} x_{ij}; \ i = 22, \ 33$$
 (4)

The energy separation between the first fundamental state and its first overtone state is expressed by Eq. (5):

$$\Delta E_{i,2\times i} = \omega_i + 4x_{i,i} + \frac{1}{2} \sum_{j \neq i}^{3N-6} x_{ij} = \nu_i + 2x_{i,i};$$

$$i = 22. 33$$
(5)

This energy separation differs from that in Eq. (4) by an additional factor of $2x_{i,i}$. Therefore, as has been done previously [40,41], the anharmonicity constant can be expressed as a function of purely experimental values, as in Eq. (6):

$$x_{i,i} = \frac{\Delta E_{i,2\times i} - \nu_i}{2}; \ i = 22, \ 33$$
 (6)

The $x_{22,33}$ constant can similarly be solved for using the equation for the experimental overtone-combination state separation, Eq. (7):

$$\Delta E_{2\times 22,22+33} = -\nu_{22} + \nu_{33} + x_{22,33} - 4x_{22,22} - 2x_{33,33} \tag{7}$$

These equations demonstrate that $x_{22,22}$, $x_{33,33}$, and $x_{22,33}$ can be determined from the fundamental band origins (ν_{22} and ν_{33}) and the hotband band origins, without necessity of knowing the summations of other anharmonicity constants. The anharmonicity constants resulting from such an analysis and the corresponding computed constants are provided in Table 7. The CCSD(T)/ANO1 value of $x_{22,22}$ is within 2.5% of the experimentally determined value, and that for $x_{22,33}$ is within 4.0%. The $x_{33,33}$ constant shows a somewhat larger discrepancy of 15.7%, but even this is quite satisfactory.

Using the experimental energies and anharmonicity constants with the computed values of $\frac{1}{2}\sum_{j\neq i}^{3N-6}x_{ij}$ in Eq. (4), it is possible to estimate semi-experimental harmonic frequencies for the ν_{22} and ν_{33} fundamentals. These values, along with comparisons of the experimentally determined term energies and computed anharmonic energies for the six vibrational states up to the ν_{21} fundamental, are provided in Table 8. In noteworthy agreement, the predicted anharmonic term energies are all within 0.5% of the experimentally determined values. Given the exemplary agreement between this level of theory and experiment for these energies and the anharmonicity constants in Table 7, it is not too surprising that the discrepancies between the semi-experimental harmonic frequencies and the CCSD(T) ones, which do require the summations of other anharmonicity constants $(\sum_{j\neq i}^{3N-6} x_{ij})$, are similarly

5. Conclusion

The combined use of millimeter-wave and high-resolution infrared spectroscopy enabled determination of not only infrared-active state energies or energy separations between interacting states, but also a complete ladder of energies for the six lowest-energy vibrationally excited states. The CCSD(T)/ANO1 level of theory employed here has proven very successful in reproducing these term energies, as well as the harmonic and anharmonic spectroscopic constants derived from them. A successful analysis of the Coriolis and Darling-Dennison couplings using an extensive spectroscopic data set for the $v_{22}=2$; $v_{22}=1$, $v_{33}=1$; and $v_{33} = 2$ triad of states, including identification of seven matched pairs of nominal interstate transitions between $v_{22} = 1$, $v_{33} = 1$ and $v_{33} = 2$, resulted in the determination of physically meaningful rotational and distortion constants and several corresponding coupling parameters. This analysis reveals that the magnitude of the resonances between v_{22} = 2 and $v_{22} = 1$, $v_{33} = 1$ is highly asymmetric with respect to those between $v_{22} = 1$, $v_{33} = 1$ and $v_{33} = 2$, which we attribute at least partially to interactions between the Coriolis and Darling-Dennison terms in the Hamiltonian. Comparison of coupling terms for the $v_{22} = 1$; $v_{33} = 1$ dyad to the Coriolis coupling terms of their first overtones and combination state strongly suggests that the higher-order coupling terms scale in a similar manner to the predictable change in G_a , namely that they are multiplied by $\sqrt{2}$ when going from the fundamental dyad to the triad. To

^b Term energies relative to the ground state used as fitting parameters.

^c Energies of states involved in Darling-Dennison interaction predicted using *xguinea*.

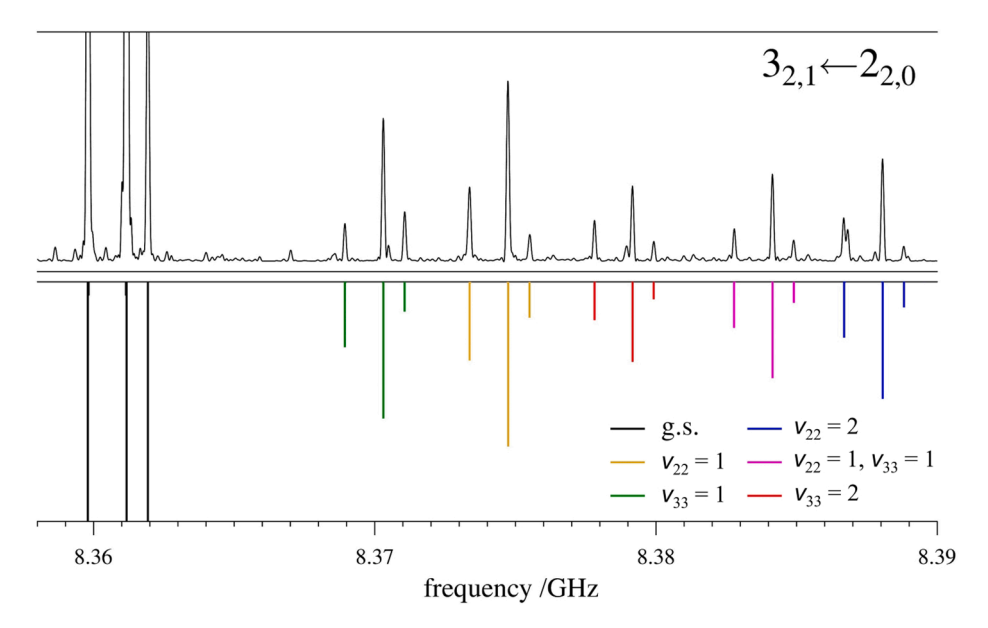


Fig. 13. Benzonitrile rotational spectrum from 8.358 to 8.390 GHz (top) and stick spectra of the ground vibrational state and five vibrationally excited states (bottom). The transitions in this frequency region are hyperfine-resolved $3_{2,1} \leftarrow 2_{2,0}$ rotational transition of each vibrational state.

the extent that this is true in general, it should prove a very useful tool in predicting these higher-order coupling terms for other molecules, which is crucial since no current computational packages predict their values. The comparisons of theory to experiment regarding the vibration-rotation interaction constants, anharmonicity constants, term energies, and harmonic frequencies at the CCSD(T)/ANO1 level of theory presented in this work show remarkable agreement with experimentally determined values, lending credence to both sets of values. A notable result is that the Darling-Dennison resonance parameter, W, is meaningfully predicted by the perturbation theory expression in Eq. (2), which is conveniently implemented in the CFOUR xguinea module. The high level of cancellation between the quartic force-constant term and the kinetic energy and cubic force-constant terms that occurs in the triad studied here may not apply to other analogous Darling-Dennison cases. Therefore, the value of W and the magnitude of its effects may be even larger for other molecules or states than it was here. While the mere 2% discrepancy between theory and experiment in this case may be partially fortuitous, the general utility of this method of prediction is clear.

Although the six-state least-squares fit of the ground vibrational state, $v_{22} = 1$; $v_{33} = 1$ dyad, and the corresponding triad shows signs of imperfection in the data distribution plots and somewhat higher-thandesirable σ value for the least-squares fit of the $v_{22} = 1$, $v_{33} = 1$ state, we present evidence of the accuracy of the determined constants. An ultimate test, of course, is the extent to which these constants can be used to predict transitions at lower frequencies, and the constants presented in this work are successful in such extrapolation. Provided in the supplementary material are the obs. - calc. values for data in the 8-18 GHz frequency region using the constants determined in the multi-state fit and the quadrupole coupling constants of the ground vibrational state. Fig. 13 shows a section from this spectral region and the extrapolated transition frequencies. The majority of transitions are predicted within the 10 kHz experimental uncertainty, demonstrating the reliability of the constants presented here. While the ground-state leastsquares fit includes transitions from such low frequencies, there are no previously published low-frequency rotational transitions for the vibrationally excited states. The only previously published spectroscopic constants for the vibrationally excited states were those for $\nu_{22}=1$ and $v_{33} = 1$ from our previous work [28]. Therefore, the ability of the determined constants to accurately extrapolate so far below the frequency region in which they were determined confirms that these constants - the rotational and distortion constants, and, importantly, the coupling terms – are reasonably close to their true values. We attribute this accuracy to the practices of including as many transitions as possible in the data set, holding constants that cannot be determined at the best available estimate of their value, and attempting to minimize convolution of coupling in the rotational and distortion constants. The spectroscopic and coupling constants determined in this work should thus provide a reliable basis for extraterrestrial identification and analysis of the six lowest-energy vibrational states of benzonitrile.

Declaration of Competing Interest

The authors declare that they have no known competing financial interests or personal relationships that could have appeared to influence the work reported in this paper.

Acknowledgments

We gratefully acknowledge funding from the U.S. National Science Foundation for support of this project (CHE-1664912 and CHE-1954270). We thank Michael McCarthy for the loan of an amplification-multiplication chain and the Harvey Spangler Award (to B.J.E.) for funding that supported purchase of the corresponding detector. M.A.Z thanks John. F. Stanton for informative discussions on Darling-Dennison resonance. M.-A.M-D. and O.P. acknowledge support from the Programme National "Physique et Chimie du Milieu Interstellaire" (PCMI) of CNRS/INSU with INC/INP co-funded by CEA and CNES.

Appendix A. Supplementary data

Supplementary data to this article can be found online at https://doi. org/10.1016/j.jms.2021.111568.

References

- P. Thaddeus, J.M. Vrtilek, C.A. Gottlieb, Laboratory and astronomical identification of cyclopropenylidene, C₃H₂, Astrophys. J. 299 (1985) L63–L66.
- [2] P. Cox, R. Guesten, C. Henkel, Observations of cyclopropenylidene in the diffuse interstellar medium, Astron. Astrophys. 206 (1988) 108–116.
- [3] J. Cernicharo, A.M. Heras, A.G.G.M. Tielens, J.R. Pardo, F. Herpin, M. Guelin, L.B. F.M. Waters, Infrared space observatory's discovery of C₄H₂, C₆H₂, and benzene in CRL 618, Astrophys. J. 546 (2001) L123–L126.
- [4] J.M. Hollis, A.J. Remijan, P.R. Jewell, F.J. Lovas, Cyclopropenone (c-H₂C₃O): a new interstellar ring molecule, Astrophys. J. 642 (2006) 933–939.

- [5] B.A. McGuire, A.M. Burkhardt, S.V. Kalenskii, C.N. Shingledecker, A.J. Remijan, E. Herbst, M.C. McCarthy, Detection of the Aromatic Molecule Benzonitrile (c-C₆H₅CN) in the Interstellar Medium, Science 359 (2018) 202–205.
- [6] M.C. McCarthy, K.L.K. Lee, R.A. Loomis, A.M. Burkhardt, C.N. Shingledecker, S. B. Charnley, M.A. Cordiner, E. Herbst, S. Kalenskii, E.R. Willis, C. Xue, A. J. Remijan, B.A. McGuire, Interstellar detection of the highly polar five-membered ring cyanocyclopentadiene, Nat. Astron. 5 (2021) 176–180.
- [7] B.A. McGuire, R.A. Loomis, A.M. Burkhardt, K.L.K. Lee, C.N. Shingledecker, S. B. Charnley, I.R. Cooke, M.A. Cordiner, E. Herbst, S. Kalenskii, M.A. Siebert, E. R. Willis, C. Xue, A.J. Remijan, M.C. McCarthy, Detection of two interstellar polycyclic aromatic hydrocarbons via spectral matched filtering, Science 371 (2021) 1265–1269.
- [8] J. Cernicharo, M. Agúndez, C. Cabezas, B. Tercero, N. Marcelino, J.R. Pardo, P. de Vicente, Pure hydrocarbon cycles in TMC-1: Discovery of ethynyl cyclopropenylidene, cyclopentadiene, and indene, A&A 649 (2021) L15.
- [9] C.A. Nixon, A.E. Thelen, M.A. Cordiner, Z. Kisiel, S.B. Charnley, E.M. Molter, J. Serigano, P.G. Irwin, N.A. Teanby, Y.-J. Kuan, Detection of cyclopropenylidene on Titan with ALMA, Astron. J. 160 (2020) 205.
- [10] P.M. Dorman, B.J. Esselman, R.C. Woods, R.J. McMahon, An analysis of the rotational ground state and lowest-energy vibrationally excited dyad of 3-cyanopyridine: Low symmetry reveals rich complexity of perturbations, couplings, and interstate transitions, J. Mol. Spectrosc. 373 (2020), 111373.
- [11] P.M. Dorman, B.J. Esselman, J.E. Park, R.C. Woods, R.J. McMahon, Millimeter-wave spectrum of 4-cyanopyridine in its ground state and lowest-energy vibrationally excited states, v₂₀ and v₃₀, J. Mol. Spectrosc. 369 (2020), 111274.
- [12] K. Wohlfart, M. Schnell, J.-U. Grabow, J. Küpper, Precise dipole moment and quadrupole coupling constants of benzonitrile, J. Mol. Spectrosc. 247 (2008) 119–121
- [13] B.N. Khare, C. Sagan, J.E. Zumberge, D.S. Sklarew, B. Nagy, Organic solids produced by electrical discharge in reducing atmospheres: Tholin molecular analysis, Icarus 48 (1981) 290–297.
- [14] N. Balucani, O. Asvany, L.C.L. Huang, Y.T. Lee, R.I. Kaiser, Y. Osamura, H. F. Bettinger, Formation of nitriles in the interstellar medium via reactions of cyano radicals, CN(X ²Σ⁺), with unsaturated hydrocarbons, Astrophys. J. 545 (2000) 892–906.
- [15] P.M. Woods, T.J. Millar, A.A. Zijlstra, E. Herbst, The synthesis of benzene in the proto-planetary nebula CRL 618, Astrophys. J. Lett. 574 (2002) L167–L170.
- [16] D.E. Woon, Modeling chemical growth processes in Titan's atmosphere: 1. Theoretical rates for reactions between benzene and the ethynyl (C₂H) and cyano (CN) radicals at low temperature and pressure, Chem. Phys. 331 (2006) 67–76.
- [17] D.S.N. Parker, R.I. Kaiser, O. Kostko, T.P. Troy, M. Ahmed, B.-J. Sun, S.-H. Chen, A. H.H. Chang, On the formation of pyridine in the interstellar medium, PCCP 17 (2015) 32000–32008.
- [18] K.B. Jefferts, A.A. Penzias, R.W. Wilson, Observation of the CN radical in the orion nebula and W51, Astrophys. J. 161 (1970) L87–L89.
- [19] B. Bak, J.T. Nielsen, Infrared absorption spectra of benzonitrile and its monodeuteriated derivatives. Tentative assignments of fundamentals, Z. Elektrochem. Angew. Phys. Chem. 64 (1960) 560–562.
- [20] J.H.S. Green, D.J. Harrison, Vibrational spectra of benzene derivatives—XVII. Benzonitrile and substituted benzonitriles, Spectrochim. Acta A 32 (1976) 1279–1286.
- [21] G. Erlandsson, Microwave spectrum of benzonitrile, J. Chem. Phys. 22 (1954) 1152.
- [22] D.J.R. Lide, Microwave spectrum and structure of benzonitrile, J. Chem. Phys. 22 (1954) 1577–1578.
- [23] B. Bak, D. Christensen, W.B. Dixon, L. Hansen-Nygaard, J. Rastrup-Andersen, Benzene ring distortion by one substituent. microwave determination of the complete structure of benzonitrile, J. Chem. Phys. 37 (1962) 2027–2031.
- [24] J. Casado, L. Nygaard, G.O. Sørensen, Microwave spectra of isotopic benzonitriles. Refined molecular structure of benzonitrile, J. Mol. Struct. 8 (1971) 211–224.
- [25] E. Fliege, G. Bestmann, R. Schwarz, H. Dreizler, Quadrupole coupling in benzonitrile. An application of microwave Fourier transform spectroscopy, Z. Naturforsch., A 36A (1981) 1124–1125.
- [26] K. Vormann, U. Andresen, N. Heineking, H. Dreizler, Quadrupole hyperfine structure in the rotational spectrum of benzonitrile, Z. Naturforsch., A: Phys. Sci. 43 (1988) 283–284.
- [27] G. Wlodarczak, J. Burie, J. Demaison, K. Vormann, A.G. Császár, The rotational spectrum of benzonitrile: Experimental and theoretical determination of the quartic centrifugal distortion constants, J. Mol. Spectrosc. 134 (1989) 297–304.
- [28] M.A. Zdanovskaia, B.J. Esselman, H.S. Lau, D.M. Bates, R.C. Woods, R.J. McMahon, Z. Kisiel, The 103–360 GHz rotational spectrum of benzonitrile, the first interstellar benzene derivative detected by radioastronomy, J. Mol. Spectrosc. 351 (2018) 39–48.
- [29] M.A. Zdanovskaia, B.J. Esselman, S.M. Kougias, A.R. Patel, R.C. Woods, R.J. McMahon, The 130 370 GHz Rotational Spectrum of syn-2-Cyano-1,3-Butadiene (C₅H₄N) A Molecule of Astrochemical Relevance, Mol. Phys. 199 (2021) 1964629.
- [30] B.J. Esselman, S.M. Kougias, M.A. Zdanovskaia, R.C. Woods, R.J. McMahon, Synthesis, purification, and rotational spectroscopy of (cyanomethylene) cyclopropane—an isomer of pyridine, J. Phys. Chem. A 125 (2021) 5601–5614.
- [31] Z. Kisiel, C.A. Nixon, M.A. Cordiner, A.E. Thelen, S.B. Charnley, Propionitrile in the two lowest excited vibrational states in the laboratory and on Titan, J. Mol. Spectrosc. 372 (2020), 111324.
- [32] M.A. Zdanovskaia, B.J. Esselman, R.C. Woods, R.J. McMahon, The 130–370 GHz rotational spectrum of phenyl isocyanide (C₆H₅NC), J. Chem. Phys. 151 (2019), 024301.

- [33] O. Pirali, Z. Kisiel, M. Goubet, S. Gruet, M.A. Martin-Drumel, A. Cuisset, F. Hindle, G. Mouret, Rotation-vibration interactions in the spectra of polycyclic aromatic hydrocarbons: Quinoline as a test-case species, J. Chem. Phys. 142 (2015), 104310.
- [34] D.W. Tokaryk, S.D. Culligan, B.E. Billinghurst, J.A. van Wijngaarden, Synchrotron-based far-infrared spectroscopy of furan: Rotational analysis of the ν_{14} , ν_{11} , ν_{18} and ν_{19} vibrational levels, J. Mol. Spectrosc. 270 (2011) 56–60.
- [35] Z. Kisiel, A. Kraśnicki, The millimetre-wave rotational spectrum of phenylacetylene, J. Mol. Spectrosc. 262 (2010) 82–88.
- [36] Z. Kisiel, E.B. Jaworska, R.A.H. Butler, D.T. Petkie, P. Helminger, I.R. Medvedev, F. C. De Lucia, The rotational spectrum of chlorine nitrate (ClONO₂) in the four lowest *nν*₉ polyads, J. Mol. Spectrosc. 254 (2009) 78–86.
- [37] Z. Kisiel, E. Białkowska-Jaworska, L. Pszczółkowski, The millimeter-wave rotational spectrum of fluorobenzene, J. Mol. Spectrosc. 232 (2005) 47–54.
- [38] B.J. Esselman, M.A. Zdanovskaia, T.K. Adkins, B.E. Billinghurst, J. Zhao, R. C. Woods, R.J. McMahon, Millimeter-wave and infrared spectroscopy of thiazole (c-C₃H₃NS) in its ground state and lowest-energy vibrationally excited states (ν₁₈, ν₁₇, and ν₁₃), J. Mol. Spectrosc. 379 (2021), 111493.
- [39] A.G. Császár, G. Fogarasi, Scaled quantum mechanical (SQM) force field and theoretical vibrational spectrum for benzonitrile, Spectrochim. Acta A 45 (1989) 845–854.
- [40] Z. Kisiel, M.-A. Martin-Drumel, O. Pirali, Lowest vibrational states of acrylonitrile from microwave and synchrotron radiation spectra, J. Mol. Spectrosc. 315 (2015) 83–91.
- [41] Z. Kisiel, M. Winnewisser, B.P. Winnewisser, F.C. De Lucia, D.W. Tokaryk, B. E. Billinghurst, Far-infrared spectrum of S(CN)₂ measured with synchrotron radiation: global analysis of the available high-resolution spectroscopic data, J. Phys. Chem. A 117 (2013) 13815–13824.
- [42] S.M. Fortman, J.P. McMillan, C.F. Neese, S.K. Randall, A.J. Remijan, T.L. Wilson, F. C. De Lucia, An analysis of a preliminary ALMA Orion KL spectrum via the use of complete experimental spectra from the laboratory, J. Mol. Spectrosc. 280 (2012) 11–20
- [43] A.M. Daly, C. Bermúdez, A. López, B. Tercero, J.C. Pearson, N. Marcelino, J. L. Alonso, J. Cernicharo, Laboratory characterization and astrophysical detection of vibrationally excited states of ethyl cyanide, Astrophys. J. 768 (2013) 81.
- [44] A. López, B. Tercero, Z. Kisiel, A.M. Daly, C. Bermúdez, H. Calcutt, N. Marcelino, S. Viti, B.J. Drouin, I.R. Medvedev, C.F. Neese, L. Pszczółkowski, J.L. Alonso, J. Cernicharo, Laboratory characterization and astrophysical detection of vibrationally excited states of vinyl cyanide in Orion-KL. A&A 572 (2014) A44.
- [45] C.P Endres, M.-A. Martin-Drumel, O. Zingsheim, L. Bonah, O. Pirali, T. Zhang, Á. Sánchez-Monge, T. Möller, N. Wehres, P. Schilke, M.C Mccarthy, S. Schlemmer, P. Caselli, S. Thorwirth, SOLEIL and ALMA views on prototypical organic nitriles: C₂H₅CN, J. Mol. Spectrosc. 375 (2021) 111392.
- [46] B.J. Esselman, B.K. Amberger, J.D. Shutter, M.A. Daane, J.F. Stanton, R.C. Woods, R.J. McMahon, Rotational spectroscopy of pyridazine and its isotopologs from 235–360 GHz: equilibrium structure and vibrational satellites, J. Chem. Phys. 139 (2013), 224304.
- [47] Z. Kisiel, E. Białkowska-Jaworska, Sextic centrifugal distortion in fluorobenzene and phenylacetylene from cm-wave rotational spectroscopy, J. Mol. Spectrosc. 359 (2019) 16–21.
- [48] M. Krüger, H. Harder, C. Gerke, H. Dreizler, An Automatic Scan Waveguide Microwave Fourier Transform Spectrometer, Z. Naturforsch. 48a (1993) 737-738.
- [49] M. Krüger, H. Dreizler, A microwave fourier transform spectrometer with a single microwave source, Z. Naturforsch. 45a (1990) 724-726.
- [50] J.B. Brubach, L. Manceron, M. Rouzières, O. Pirali, D. Balcon, F.K. Tchana, V. Boudon, M. Tudorie, T. Huet, A. Cuisset, P. Roy, Performance of the AILES THZ-Infrared beamline at SOLEIL for high resolution spectroscopy, AIP Conf. Proc. 1214 (2010) 81–84.
- [51] O. Pirali, V. Boudon, J. Oomens, M. Vervloet, Rotationally resolved infrared spectroscopy of adamantane, J. Chem. Phys. 136 (2012), 024310.
- [52] V.-M. Horneman, High accurate peak positions for calibration purposes with the lowest fundamental bands ν_2 of N₂O and CO₂, J. Mol. Spectrosc. 241 (2007) 45–50.
- [53] V.M. Horneman, R. Anttila, S. Alanko, J. Pietilä, Transferring calibration from CO₂ laser lines to far infrared water lines with the aid of the ν₂ band of OCS and the ν₂, ν₁-ν₂, and ν₁+ν₂ bands of ¹³CS₂; Molecular constants of ¹³CS₂, J. Mol. Spectrosc. 234 (2005) 238-254.
- [54] F. Matsushima, H. Odashima, T. Iwasaki, S. Tsunekawa, K. Takagi, Frequency measurement of pure rotational transitions of $\rm H_2O$ from 0.5 to 5 THz, J. Mol. Struct. 352–353 (1995) 371–378.
- [55] Z. Kisiel, L. Pszczółkowski, B.J. Drouin, C.S. Brauer, S. Yu, J.C. Pearson, I. R. Medvedev, S. Fortman, C. Neese, Broadband rotational spectroscopy of acrylonitrile: Vibrational energies from perturbations, J. Mol. Spectrosc. 280 (2012) 134–144.
- [56] Z. Kisiel, L. Pszczółkowski, I.R. Medvedev, M. Winnewisser, F.C. De Lucia, E. Herbst, Rotational spectrum of *trans-trans* diethyl ether in the ground and three excited vibrational states, J. Mol. Spectrosc. 233 (2005) 231–243.
- [57] W. Łodyga, M. Kręglewski, P. Pracna, Š. Urban, Advanced graphical software for assignments of transitions in rovibrational spectra, J. Mol. Spectrosc. 243 (2007) 182–188.
- [58] Z. Kisiel, Assignment and analysis of complex rotational spectra, in: J. Demaison, K. Sarka, E.A. Cohen (Eds.), Spectroscopy from Space, Kluwer Academic Publishers, Dordrecht, 2001, pp. 91-106; http://www.ifpan.edu.pl/~kisiel/prospe.htm.
- [59] Z. Kisiel, PROSPE—Programs for ROtational SPEctroscopy. http://info.ifpan.edu.pl/~kisiel/prospe.htm. (accessed 2021).
- [60] H.M. Pickett, The fitting and prediction of vibration-rotation spectra with spin interactions, J. Mol. Spectrosc. 148 (1991) 371–377.

- [61] J.F. Stanton, J. Gauss, L. Cheng, M.E. Harding, D.A. Matthews, P.G. Szalay, CFOUR, Coupled-Cluster Techniques for Computational Chemistry, with contributions from A. A. Auer, R. J. Bartlett, U. Benedikt, C. Berger, D. E. Bernholdt, S. Blaschke, Y. J. Bomble, S. Burger, O. Christiansen, D. Datta, F. Engel, R. Faber, J. Greiner, M. Heckert, O. Heun, M. Hilgenberg, C. Huber, T.-C. Jagau, D. Jonsson, J. Jusélius, T. Kirsch, K. Klein, G. M. Kopper, W. J. Lauderdale, F. Lipparini, T. Metzroth, L. A. Mück, T. Nottoli, D. P. O'Neill, D. R. Price, E. Prochnow, C. Puzzarini, K. Ruud, F. Schiffmann, W. Schwalbach, C. Simmons, S. Stopkowicz, A. Tajti, J. Vázquez, F. Wang, J. D. Watts and the integral packages MOLECULE (J. Almlöf and P. R. Taylor), PROPS (P. R. Taylor), ABACUS (T. Helgaker, H. J. Aa. Jensen, P. Jørgensen, and J. Olsen), and ECP routines by A. V. Mitin and C. van Wüllen, http://www.cfour.de.
- [62] I.M. Mills, Infrared spectra. Vibration-rotation structure in asymmetric- and symmetric-top molecules, in: K.N. Rao, C.W. Mathews (Eds.), Molecular Spectroscopy: Modern Research, Academic Press, New York, 1972, pp. 115–140.
- [63] J.F. Stanton, C.L. Lopreore, J. Gauss, The equilibrium structure and fundamental vibrational frequencies of dioxirane, J. Chem. Phys. 108 (1998) 7190–7196.
- [64] U. Dahmen, W. Stahl, H. Dreizler, The rotational spectrum of the benzonitrileargon van der Waals complex, Ber. Bunsenge. Phy. Chem. 98 (1994) 970–974.

- [65] H.D. Rudolph, J. Demaison, A.G. Csaszar, Accurate Determination of the Deformation of the Benzene Ring upon Substitution: Equilibrium Structures of Benzonitrile and Phenylacetylene, J. Phys. Chem. A 117 (2013) 12969–12982.
- [66] Z. Kisiel, E. Bialkowska-Jaworska, L. Pszczólkowski, The mm-wave rotational spectrum of CBrClF₂ (Halon BCF): observation of a new R-type band and generalization of conditions for oblate-type band formation, J. Mol. Spectrosc. 177 (1996) 240–250.
- [67] Z. Kisiel, L. Pszczółkowski, Assignment and analysis of the mm-wave rotational spectrum of trichloroethylene: observation of a new, extended ^bR-band and an overview of high-J, R-type bands, J. Mol. Spectrosc. 178 (1996) 125–137.
- [68] D. Papoušek, M.R. Aliev, Molecular Vibrational-rotational Spectra: Theory and Applications of High Resolution Infrared, Microwave, and Raman Spectroscopy of Polyatomic Molecules, Elsevier Scientific Publishing Company, 1982.
- [69] J indicates that $K_a + K_c = J$, and J+1 indicates that $K_a + K_c = J + 1$.
- [70] B.T. Darling, D.M. Dennison, The water vapor molecule, Phys. Rev. 57 (1940) 128–139.
- [71] D.A. Matthews, J. Vázquez, J.F. Stanton, Calculated stretching overtone levels and Darling-Dennison resonances in water: a triumph of simple theoretical approaches, Mol. Phys. 105 (2007) 2659–2666.